Author's Accepted Manuscript

www.elsevier.com/locate/jmbbm

A mechanistic insight into the mechanical role of the *stratum corneum* during stretching and compression of the skin.

Maria F. Leyva-Mendivil, Anton Page, Neil W. Bressloff, Georges Limbert

PII: S1751-6161(15)00174-5
DOI: http://dx.doi.org/10.1016/j.jmbbm.2015.05.010
Reference: JMBBM1478

To appear in: *Journal of the Mechanical Behavior of Biomedical Materials*

Received date: 10 February 2015
Revised date: 30 April 2015
Accepted date: 12 May 2015

Cite this article as: Maria F. Leyva-Mendivil, Anton Page, Neil W. Bressloff, Georges Limbert, A mechanistic insight into the mechanical role of the *stratum corneum* during stretching and compression of the skin., *Journal of the Mechanical Behavior of Biomedical Materials,* http://dx.doi.org/10.1016/j.jmbbm.2015.05.010

A mechanistic insight into the mechanical role of the *stratum corneum* during stretching and compression of the skin.

Maria F. Leyva-Mendivil [1,2], **Anton Page** [3], **Neil W. Bressloff** [4] **and Georges Limbert** [1,2,5 *]

[1]national Centre for Advanced Tribology at Southampton (nCATS), Faculty of Engineering and the Environment, University of Southampton. Southampton, SO17 1BJ, UK.
[2]Bioengineering Research Group, Faculty of Engineering and the Environment, University of Southampton. Southampton, SO17 1BJ, UK.
[3]Biomedical Imaging Unit, Southampton General Hospital. Southampton, SO16 6YD, UK.
[4]Computational Engineering and Design Group, Faculty of Engineering and the Environment, University of Southampton. Southampton, SO17 1BJ, UK.
[5]Division of Biomedical Engineering, Department of Human Biology, Faculty of Health Sciences, University of Cape Town, Observatory 7935, South Africa.

Abstract

The study of skin biophysics has largely been driven by consumer goods, biomedical and cosmetic industries which aim to design products that efficiently interact with the skin and/or modify its biophysical properties for health or cosmetic benefits. The skin is a hierarchical biological structure featuring several layers with their own distinct geometry and mechanical properties. Up to now, no computational models of the skin have simultaneously accounted for these geometrical and material characteristics to study their complex biomechanical interactions under particular macroscopic deformation modes.

The goal of this study was, therefore, to develop a robust methodology combining histological sections of human skin, image-processing and finite element techniques to address fundamental questions about skin mechanics and, more particularly, about how macroscopic strains are transmitted and modulated through the epidermis and dermis. The work hypothesis was that, as skin deforms under macroscopic loads, the *stratum corneum* does not experience significant strains but rather folds/unfolds during skin extension/compression.

A sample of fresh human mid-back skin was processed for wax histology. Sections were stained and photographed by optical microscopy. The multiple images were stitched together to produce a larger region of interest and segmented to extract the geometry of the *stratum corneum*, viable epidermis and dermis. From the segmented structures a 2D finite element mesh of the skin composite model was created and geometrically non-linear plane-strain finite element analyses were conducted to study the sensitivity of the model to variations in mechanical properties.

The hybrid experimental-computational methodology has offered valuable insights into the simulated mechanics of the skin, and that of the *stratum corneum* in particular, by providing qualitative and quantitative information on strain magnitude and distribution.
Through a complex non-linear interplay, the geometry and mechanical characteristics of the skin layers (and their relative balance), play a critical role in conditioning the skin mechanical response to macroscopic in-plane compression and extension. Topographical features of the skin surface such as furrows were shown to act as an efficient means to deflect, convert and redistribute strain—and so stress—within the *stratum corneum*, viable epidermis and dermis. Strain reduction and amplification phenomena were also observed and quantified.

Despite the small thickness of the *stratum corneum*, its Young's modulus has a significant effect not only on the strain magnitude and directions within the *stratum corneum* layer but also on those of the underlying layers. This effect is reflected in the deformed shape of the skin surface in simulated compression and extension and is intrinsically linked to the rather complex geometrical characteristics of each skin layer. Moreover, if the Young's modulus of the viable epidermis is assumed to be reduced by a factor 12, the area of skin folding is likely to increase under skin compression. These results should be considered in the light of published computational models of the skin which, up to now, have ignored these characteristics.

Key words

Skin, *stratum corneum*, epidermis, dermis, finite element, strain

Journal:	Journal of the Mechanical Behavior of Biomedical Materials
Article type:	Research Article [**Revision 1**]
Date:	30 April 2015
***Corresponding author:**	Tel: +44 (0)2380 592381; fax: +44 (0)2380 593016. E-mail address: g.limbert@soton.ac.uk

1 Introduction

In the last few decades, the study of skin biophysics has largely been driven by pharmaceutic, cosmetic and consumer goods industries which aim to offer solutions to reduce the effects of intrinsic and extrinsic ageing factors on skin health and appearance (e.g. using topical agents) and to design products that efficiently interact with the skin (e.g. razors). The surface of the human skin is characterised by ridged features, or skin furrows (*sulci cutis*), varying in length between 70 and 200µm for the main furrows and 20 and 70µm for the superficial furrows (Piérard et al., 2004; Shimizu, 2007). These furrows, which represent the natural microrelief of the skin, along with natural or muscle-induced wrinkles, are thought to deflect tensional forces thus providing mechanical advantages to the skin (Pedersen & Jemec, 2006). As skin deforms under macroscopic loads it is unclear whether the *stratum corneum* experiences significant local strains (change of length) or simply unfolds/folds during skin extension/compression as suggested by Geerligs (2010). Providing a mechanistic quantitative insight into this question constitutes the main objective of the present study for which an image-based anatomical modelling approach is developed. Understanding the role of the skin microstructure on its response to deformations has the potential to shed light on fundamental questions such as evolutionary aspects concerning the advantages provided by certain skin characteristics or functional abilities. For example, it was recently demonstrated that water-induced finger wrinkles in humans improved the handling of submerged objects (Kareklas et al., 2013), therefore confirming a possible evolutionary mechanical advantage for manipulating objects in submerged conditions (Changizi et al., 2011). An in-depth understanding of the structure-function relationship of the skin also presents many opportunities for practical applications in the aforementioned industrial sectors besides the obvious applications in biomedical and health sciences where the coupling between mechanics and biology (i.e. mechanobiology) is particularly relevant (Brand, 2006).

Being the outermost of the skin layers, the *stratum corneum* is the prime line of defence against environmental threats being they mechanical, thermal, chemical, radiological or biological. Epithelial cells structuring the epidermis replicate in the basal layer and progressively migrate towards the surface of the skin effectively ensuring the regenerative nature of this fundamental layer. In this process, the structure of cells changes as they get deprived of nutrients provided by blood vessels that do not extend beyond the basal layer. The cells eventually die, release their glycolipids into the intracellular space, become flat and finally keratinise to form the *stratum corneum* (Marieb and Hoehn, 2010; Shimizu, 2007). These strong keratinised cells, bonded by desmosomes, form the so-called "brick and mortar" structure (Derler and Gerhardt, 2012; Geerligs et al., 2011) that characterises the *stratum corneum* as a stiff mechanical barrier. In a biotribological context, the nature of physical interactions between the skin and the external environment is strongly conditioned by the propensity of the *stratum corneum* to absorb liquids such as water and lubricants (Bhushan, 2012; Wu et al., 2006) which modify its mechanical and chemical properties, which in turn affect the physical appearance of the skin surface (Raab, 1990) and its mechanical response to deformations. This is due to its complex multi-scale structure, (time-dependent) intrinsic mechanical properties and the nature of its structural and mechanobiological interactions with other skin constituents such as the viable epidermis and underlying dermis.

The sensitivity of the mechanical characteristics of the *stratum corneum* to environmental conditions, particularly relative humidity, is well established (Dauskardt et al., 2011; Dauskardt et al., 2006; Levi and Dauskardt, 2010; Levi et al., 2010; Pailler-Mattei et al., 2007; Wu et al., 2002, 2006) and references therein. This phenomenon results in significant intra-sample variability of its mechanical properties. Typically, the Young's modulus of the *stratum corneum* decreases with relative humidity because of the water-induced plasticisation effect affecting its "brick and mortar" structure. Moreover, differences in experimental measurement techniques, testing conditions, inter-and intra-subject variability are translated into a wide range of mechanical properties found in the literature (**Table 1**) and this variability must be considered in models if one wants to obtain more universal results. In a finite element modelling context, it implies that using a single set of mechanical properties for the *stratum corneum* would limit the domain of validity of the simulation results to specific conditions.

A wide array of experimental and clinical measurement techniques are used to characterise particular aspects of skin biology and biophysics (Alexiades-Armenakas, 2007; Batisse et al., 2002; Bellemere et al., 2009; Delalleau et al., 2006; Diridollou et al., 2000; Gunner et al., 1979; Hendriks et al., 2006; Jor et al., 2013; Limbert and Simms, 2013; Tonge et al., 2013a; Tonge et al., 2013b; Wan Abas, 1994). Nevertheless, complementary approaches based on mathematical and computational modelling techniques offer promising avenues to further our understanding of the skin (Areias et al., 2003; Bischoff et al., 2000; Boissieux et al., 2000; Buganza Tepole and Kuhl, 2014; Cavicchi et al., 2009; Duan et al., 2000; Evans, 2009; Flynn and McCormack, 2008a, b; Flynn and McCormack, 2009, 2010; Hendriks et al., 2006; Hendriks et al., 2003; Kuwazuru et al., 2008; Larrabee, 1986; Larrabee and Galt, 1986a, b; Larrabee and Sutton, 1986; Lévêque and Audoly, 2013; Tepole et al., 2014a; Tepole et al., 2014b; Tepole et al., 2011; Zöllner et al., 2013).

These methods have the potential to provide a mechanistic insight into the role and interplay of the material and structural properties of the different skin constituents, albeit in simplified idealised conditions. A microstructural outlook on the mechanics of skin can be exploited to design innovative cosmetic and consumer good products. For example, by locally controlling the stiffness of skin layers using targeted nanoparticles one could ultimately modify the skin topography (wrinkles) and therefore its appearance (Limbert, 2014). Moreover, modelling approaches can be used to complement physical and clinical experiments by guiding their design (Hendriks et al., 2006; Hendriks et al., 2003). Intra-individually, the biological and mechanical characteristics of skin, considered either as a material or a composite structure, are also known to vary with age (Waller and Maibach, 2005, 2006), environmental conditions (Wilhelm et al., 1991), hormonal changes (Bolognia et al., 1989) and exposure to specific chemical agents (Dauskardt et al., 2010, 2011; Matts et al., 2006).
The experimental characterisation of mechanical strains inside and at the external surface of the *stratum corneum* is a tremendous technical challenge due to its sensitivity to environmental conditions, size, limitations of existing metrology technologies, experimental measurement errors and issues of repeatability. The approach proposed in this article is a prime example of where a physics-based modelling study can address simple fundamental questions unavailable by other means. To reach this goal, what is required is basic information about the geometry, mechanical properties and loading/boundary conditions of what is effectively a multi-component structure. Naturally, in the modelling process, and by definition, a number of simplifying assumptions and discretisation errors are introduced. However, even in the absence of experimental validation, mathematical and computational simulation tools are well suited to provide *relative* answers—the so-called "what if scenarios": how one or several parameters of the system can affect its output response.

The central focus of the present study is to test the hypothesis that, in a two-dimensional (2D) modelling context, as skin deforms under macroscopic loads, the local strains experienced by the *stratum corneum* are modulated by the effect of its geometry and material properties. We propose to identify and quantify potential mechanisms by which strains in the *stratum corneum* are reduced or amplified with respect to global macroscopic strains. This aim is achieved through the key objective of assessing the magnitude and distributions of strains induced in the *stratum corneum*, viable epidermis and dermis in a simplified anatomically-based 2D model as a result of simulated in-plane compression and extension of the skin. Particular attention is paid to evaluating the interplay between the mechanical properties of each layer and the relationship between macroscopic and local strains. The study provides an opportunity to highlight potentially important anatomical structural effects that are missed by idealised multi-layer models of the skin.

In order to capture a wider range of conditions the finite element analyses presented in this study consider extreme values for the mechanical properties of the *stratum corneum*. In the next section, a methodology combining histology, image processing and finite element modelling to analyse the mechanical behaviour of a three-layer model of the skin (*stratum corneum*, viable epidermis and dermis) is described. This approach brings a new level of anatomical fidelity which is a stepping stone in the state-of-the-art modelling of human skin. To indirectly account for the sensitivity of the *stratum corneum* to relative humidity, a series of parametric finite element analyses varying the properties of the *stratum corneum* are conducted. Results of the analyses are presented in the third section and discussed in the fourth section.

2 Materials and methods

2.1 Skin histology and imaging

A fresh mid-back skin sample was obtained from a 30 years-old healthy white Caucasian female patient following biopsy. The specimen was processed, sliced, stained (haematoxylin and eosin) and stored by the Biomedical Imaging Unit (BIU) at Southampton General Hospital under given consent for its use for research by the patient. The use of images obtained from the histology sections for the development of this model was ethically approved by both the Research Governance Office at the University Hospital Southampton NHS foundation Trust, Research and Development department (ID: RHM MISC0014, December 6th, 2013), and the Ethics and Research Governance at University of Southampton (ID: 6751, October 10th, 2013).
A microscope adapted with a Nikon E950 camera (Nikon UK Ltd, Kingston Upon Thames, UK) was used to obtain the images of the histology sections. A series of images (1600 x 1200 pixels, JPG format with maximum quality settings) was taken for each section at automatic aperture and exposure time, ISO-80 speed, no flash, at both 4X and 10X magnifications, including the images of the scale bar which were later used for dimensioning the model. For better resolution of the skin topography, only the 10 X magnification images of each section were manually stitched together in a software environment (GIMP, www.gimp.org) by aligning each image with the next one, ensuring the overlapping parts correctly matched, forming a single PNG image (**Figure 1**).

2.2 Image processing and finite element meshing

The single PNG image of the combined skin histological sections was processed in order to develop a 2D anatomical model of the skin capturing not only the skin topography but also the epidermal-dermal junction and the interface between the viable epidermis and the papillary dermis. The image was processed in the open-source software ImageJ 1.47v (Wayne Rasband, National Institutes of Health, USA) to enhance its contrast and then transferred into the image-processing software application ScanIP™ 6.0 (Simpleware Ltd, Exeter, UK) for segmentation. Image segmentation involved extracting the regions corresponding to the 2D boundaries and inside of each skin layer phase. This process was semi-automatically performed by a human operator using a threshold filtering algorithm which allowed segmentation of regions of interest according to pixel intensity. The clarity and contrast of the photograph was pivotal in distinguishing the different skin structures. In order to limit the model to only three phases, namely the *stratum corneum*, viable epidermis and dermis, threshold filtering was complemented by "manual" painting of the region of interest, therefore ignoring heterogeneities within each phase. A 1.93 mm long section of the skin was selected to build a representative composite model of the skin. Within the same software environment, this section was subsequently meshed into bilinear triangular finite elements. An adaptive mesh refinement algorithm was used to accurately capture the complex geometry of the skin substructures whilst minimising the total number of elements. A mesh sensitivity analysis was performed. The best compromise between accuracy of results and computing time was found for characteristic element lengths ranging from 2 to 150 µm, resulting in a total of 173,929 elements. The adaptive meshing algorithm preserves the topology of surfaces and creates a smooth mesh with low element distortion regardless of the complexity and aspect ratios of the underlying 2D structures (**Figure 2**). The overall segmentation and meshing procedure is conceptualised in **Figure 3**. The finite element mesh was then exported to the finite element analysis package Abaqus/CAE/Standard 6.13 (Simulia, Dassault Systèmes, Providence, RI, USA) for preparation of the finite element models described in **section 2.3**.

2.3 Finite element models and analyses

Preparation of the finite element model comprised definition of the material properties of each sub-structure (that is, *the stratum corneum*, viable epidermis and papillary dermis), assignment of the boundary and loading conditions and specification of potential self-contact interaction for the *stratum corneum* due to surface folding. Perfect bonding was assumed between adjacent layers. Symmetry boundary conditions were enforced at the bottom (horizontal) and left (vertical) edges of the skin model (**Figure 4**). Static finite element analysis was conducted wherein no time-dependent effects such as inertia or viscoelasticity were considered. A series of finite element models featuring distinct combinations of mechanical properties of the *stratum corneum* and/or the viable epidermis was devised. The characteristics of these models are presented in the next section. For each finite element model two analyses were considered. In-plane 20 % compression and extension of the skin surface was replicated in the finite element model by applying a lateral displacement on the free edge on the vertical right side of the model (**Figure 4**). An hybrid plane–strain 3-noded element formulation was used (CPE3H element in Abaqus) to cope with the nearly incompressible behaviour of the materials (when the Poisson's ratio is close to 0.5) which would result in locking of elements (Belytschko et al., 2000).

2.4 Mechanical properties of skin

The mechanical properties of the different skin layers have been reported by numerous authors with a wide range of variation depending on body location, hydration, age and testing techniques (**Table 1**). In most of these studies, each skin layer or the entire skin—considered as a homogeneous material—is assumed to obey an isotropic Hookean elasticity law. For example, Geerligs et al. (2011) have determined the Young's modulus of the *stratum corneum* to be 0.6 MPa while Lévêque and Audoly (2013) and Magnenat-Thalmann et al. (2002) have used values of 1-12 MPa for the Young's modulus of the *stratum corneum*, 0.05 MPa for that of the viable epidermis and 0.6 MPa for the modulus of the dermis in mathematical and computational models of skin wrinkles. With increased hydration, the elastic modulus of the *stratum corneum* can vary from about 5 MPa to 1000 MPa in the in-plane direction (parallel to the skin surface), and from about 1 MPa to 25 MPa in the out-of-plane direction. Wu et al. (2006) reported a tensile Young's modulus of 3 MPa at 100% relative humidity (RH) to 370 MPa at 30% RH. Although some authors have developed computational models of the skin (Groves et al., 2013; Limbert, 2011; Ní Annaidh et al., 2012) or the dermis (Flynn and McCormack, 2009, 2010) which account for the anisotropic properties induced by the presence of collagen fibres, this approach is not followed in the current research for two main reasons. The first reason is motivated by the decision to keep the model as simple as possible to facilitate the interpretation of results and to focus on structural rather than material effects. Secondly, the use of a continuum fibre-reinforced hyperelastic model (Holzapfel et al., 2000; Limbert, 2011; Limbert and Taylor, 2002; Weiss et al., 1996) entails the definition of a unit vector field corresponding to the local orientation of collagen fibres. It is possible to extract this information from histological sections by statistical analysis of pixels (Elbischger et al., 2004) but, in the absence of accurate structural information, any deviation from the real collagen bundle orientations might lead to very different results.

In the present 2D case, any out-of-plane fibre orientation would not be captured. In order to account for a wider range of conditions, the finite element analyses presented in this study consider extreme values for the mechanical properties of the *stratum corneum* (**Table 2**).

One of the key objectives of the present study is to assess strain magnitudes in the skin layers as a result of simulated in-plane compression and extension (apparent macroscopic strain of the whole skin composite structure of up to 20%). It is therefore critical to account for potentially large strains in each of these structures. Hookean elasticity is not appropriate for materials undergoing large deformations and the simplest alternative constitutive law valid for finite deformations is the so-called neo-Hookean elasticity. It is based on the definition of a strain energy function depending on invariants of a deformation tensor which is chosen here as the right Cauchy-Green deformation tensor $\mathbf{C}$ (Ogden, 1984). The neo-Hookean hyperelastic strain energy potential ψ is defined with the first deviatoric invariant of $\mathbf{C}$, $\overline{I}_1 = J^{-\frac{2}{3}}(\mathbf{C}:\mathbf{1})$ where $J = \sqrt{\det(\mathbf{C})}$ (varying between 0 and 1) provides a measure of material compressibility. When $J = 1$, the material is fully incompressible which implies that no change of volume is allowed and the material can only change its shape by shear deformations.

$$\psi = c_{10}(\overline{I}_1 - 3) + \frac{\kappa_0}{2}(J-1)^2 \tag{1}$$

The constitutive parameters c_{10} and κ_0 correspond, respectively, to half the shear modulus and bulk modulus of an isotropic linear elastic material because linearised neo-Hookean elasticity is equivalent to isotropic linear Hookean elasticity (Ogden, 1984). One can therefore express c_{10} and κ_0 as functions of the initial Young's modulus E and Poisson's ratio ν:

$$c_{10} = \frac{E}{4(1+\nu)} \text{ and } \kappa_0 = \frac{E}{4(1-2\nu)} \tag{2}$$

A finite element model considering the skin as a monolayer material (the three layers have the same material properties) was implemented in order to serve as a reference for subsequent comparison purposes, thus highlighting potential structural effects arising only from the surface topography. The effect of varying the *stratum corneum* properties (to simulate property variability or change in relative humidity) was addressed by two cases: **A)** the viable epidermis and dermis have identical mechanical properties; and **B)** the viable epidermis is much softer than the underlying dermis (**Table 2**). For each loading case (20 % compression and 20% extension), a total of eight finite element analyses were run. For further analyses, the geometry of the skin composite model was virtually split into zones of interest corresponding to particular topographic features (**Figure 5**) which will be discussed later in the manuscript (**section 3.4**).

3 Results

Colour plots of *minimum* principal strains distributions in the skin composite model are provided in **Figure 6** and **Figure 7**, respectively for cases A and B in *compression* whilst **Figure 8** and **Figure 9** depict the *maximum* principal strains for the *extension* case (also for cases A and B). Complex non-uniform strain distribution patterns are observed for all analyses (compression and extension), thus highlighting the importance of the geometrical characteristics of each skin layer in combination with their respective mechanical properties. It is worthy to highlight that for the four cases A1-A4, the mechanical properties of the viable epidermis and dermis remained identical ($E_{VE} = E_D = 0.6$ MPa, $\nu_{VE} = \nu_D = 0.3$), only the mechanical properties of the *stratum corneum* were varied. For the four cases B1-B4, the Young's modulus of the viable epidermis was changed from 0.6 to 0.05 MPa and the mechanical properties of the *stratum corneum* were varied in the same way as they were for cases A1-A4.

3.1 Effects of mechanical properties on skin surface topography

For a fixed Poisson's ratio of the *stratum corneum*, the surface topography of the skin is clearly affected by change in stiffness of this layer.

In compression, it has the effect of reducing the self-contact area of the *stratum corneum* as two cavities resulting from the closure of the deep furrows can be observed in **Figure 6** and **Figure 7** (these deep furrows correspond to zones B and H depicted on **Figure 5**). Compared to cases A1-A4, an increase in the folding-induced contact area is observed by reducing the Young's modulus of the viable epidermis (case B, shown in **Figure 7**).

In extension, the effects are particularly visible on the deformed deep furrows which take a sharper angular shape when the highest Young's modulus is considered (**Figure 8** and **Figure 9**). The outer geometry of the skin gets softer by reducing the Young's modulus of the viable epidermis (case B, shown in **Figure 9**), provided the *stratum corneum* has its lowest stiffness ($E_{SC} = 0.6$ MPa). Varying the Poisson's ratio of the *stratum corneum* for a given Young's modulus does not have a major effect on the geometry of the deformed skin model in neither cases A and B.

3.2 Strain distribution and magnitude in the skin layers for the compression case

For a given Poisson's ratio, increasing the elastic modulus of the *stratum corneum* induces a significant redistribution of principal strains in the underlying layers: larger compressive strains are observed under compression in the viable epidermis and dermis (**Figure 6** and **Figure 7**). The effect is less apparent in the dermis when the Young's modulus of the living epidermis is about an order of magnitude smaller than that of the *stratum corneum* (cases B1-B4, **Figure 7**). However, for these cases, and as expected, the tensile strains in the viable epidermis are an order of magnitude higher. Approximately 30% compressive strains are produced in the viable epidermis zones interdigitating with the papillae of the papillary dermis, mainly in areas surrounding and beneath skin furrows. For cases A (**Figure 6**), the area of high compressive strains extends laterally while for case B (**Figure 7**), high compressive strains are produced in the viable epidermis with further concentrations in the dermis beneath deep furrows. The difference observed between high strain levels at the bottom of furrows and low strain levels at the top of the surrounding crests reveals a potentially interesting strain deflection mechanism that could occur as a result of stiffening of the *stratum corneum* [e.g. drying stress, (Levi and Dauskardt, 2010; Levi et al., 2010)].

3.3 Strain distribution and magnitude in the skin layers for the extension case

Increasing the Young's modulus of the *stratum corneum* from 0.6 to 370 MPa has the effect of significantly altering the distribution of tensile strains in the skin in the vicinity of furrows.

Higher strain levels are observed in the viable epidermis, but the effect is less apparent in the dermis when the Young's modulus of the viable epidermis is about an order of magnitude smaller than that of the *stratum corneum* (case B, **Figure 9**), showing no significant effect in the rather homogeneous tensile strain distribution and magnitude in the dermis. In contrast, tensile strains above 50% are produced in the viable epidermis zones interdigitating with the papillae of the papillary dermis. Altering the Poisson's ratio of the *stratum corneum* has a minimal effect on the strain distribution and magnitude in the viable epidermis and dermis (compare cases B1/B3 and B2/B4, **Figure 9**).

3.4 Quantitative analysis of strains in the *stratum corneum*

The distribution of strain within the composite model of skin is intrinsically conditioned by the specific geometry of each layer of the skin sample used in this study as well as their respective mechanical properties. In order to make the analysis of results more universal, the geometry of the skin composite model was virtually split into zones of interest corresponding to characteristic surface topographic features which can be found on any human skin sample (**Figure 5-c**). These zones were selected based on geometrical features (**Figure 5-c**) but also according to trends in the distribution of principal strains in the three layers along the skin sample (**Figure 5–a-b**).

The crests and furrows were identified with the labels A-L, omitting intentionally the letter I to prevent any typographic confusion. **Crests** are labelled as A, C, E, G, J and L. The dimensions of the skin furrows were measured using the image processing software application ImageJ (U. S. National Institutes of Health, Bethesda, Maryland, USA) by measuring the distance between the deepest point in the furrow and the midpoint located between the furrow boundaries (**Figure 20**). Furrows were classified according to their depth as **deep** (B, H), **superficial** (F, K) and **wide furrows** (D) (Piérard et al., 2004; Shimizu, 2007).

The median values of the principal strains of the finite elements (evaluated at their centroid) **contained in each of the topographic regions of the** ***stratum corneum*** were extracted from the results of the finite element analyses. These metrics are defined as **local median strain** (LMS), local because they are specific to each topographical zone (**Figure 5-c**). A **global median strain** (GMS) is also defined as the median value of the strains of all of the finite elements of the *stratum corneum* layer. The rationale for defining these measures was to look at how certain topographic features of the skin surface (**Figure 5**) might amplify or reduce local strains in the *stratum corneum* in response to macroscopic deformations such as those applied during in-plane extension/compression of the skin. GMS values are explored in **Figure 10-Figure 13** while **Figure 14**-**Figure 17** report LMS values.

Figure 10 and **Figure 11** show the **median minimum principal strains** for cases A and B, respectively, **in compression**. Likewise, **Figure 12** and **Figure 13** report the median values for the **maximum principal strains** in **extension**. For a fixed Poisson's ratio, increasing the Young's modulus of the *stratum corneum* from 0.6 to 370 MPa (this is an increase by approximately a factor of 617) reduces strain levels in the *stratum corneum* by about one order of magnitude. This suggests that non-linear effects are at play here and the geometrical characteristics of the topographic features may play a significant role on strain distribution. While most of the crests show similar strain levels, the distribution of median strains in the skin furrows is not uniform. Furthermore, the level of strain across the topographic features is also affected by the stiffness of the *stratum corneum*: when the Young's modulus of the *stratum corneum* is minimal a broader strain range is observed.

3.5 Global and local strains in the *stratum corneum* for the compression case

Under **compression**, for case A, compressive strains (minimum principal strains) of maximum magnitude are observed in the superficial furrow zone F. The maximum magnitude is 19.18% (9.85% GMS) for case A1 (E_{SC} = E_D 0.6 MPa, ν_{SC} = 0.3) (**Figure 10-a**). For a stiffer stratum corneum (**Figure 10-b**), the LMS level in zone F peaks at about 1%. Similar strain levels can be observed in furrow zones B, D and H for a soft stratum corneum (cases A1 and A3), but for a stiffer *stratum corneum* intermediate values between the GMS and furrow F LMS are observed in furrow zones D, H and K. Lower magnitude of LMS levels are observed in crest features for all cases (A1, A2, A3 and A4) (**Figure 10**).

Under **compression**, variation of the Poisson's ratio of the *stratum corneum* has a small effect on the overall median strains. However, its effect is not evenly distributed along the topographic features (zones A to L). It was found that in **all crests** the strain magnitude is higher when the Poisson's ratio is maximum (ν = 0.45). For the **deep furrows zones** (B and H), the effect is reversed (the strain magnitude is lower for maximum Poisson's ratio). For **smaller furrows**, their behaviour is dependent on the *stratum corneum*'s stiffness. An inversely proportional strain-Poisson's ratio relationship for superficial furrows (F and K) and a proportional one for the shallow furrow (D) are observed for a low stiffness *stratum corneum* (**Figure 10-a**) while this behaviour is reversed in the case of a stiffer *stratum corneum* (**Figure 10-b**).

For case B, where the viable epidermis is the softest (E_{VE} = 0.05 MPa), compressive strains are maximum in the deep furrow zone **H**, with a LMS=-6.3% for the soft *stratum corneum* (2.46% GMS) (**Figure 11-a**) and -0.55% for the stiffer one (2.72% GMS) (**Figure 11-b**). Similarly to case A (**Figure 11-b**), higher levels of strain are observed in the crests when the Poisson's ratio of the *stratum corneum* is increased from 0.3 to 0.45.

For the furrows, it is observed that for the case of a soft *stratum corneum*, most of the furrows (with the exception of superficial furrow K) show a reduction in LMS as the *stratum corneum*'s Poisson's ratio increases, while for a stiffer *stratum corneum*, LMS increase with Poisson's ratio. For the stiffest *stratum corneum* (**Figure 10-b**, **Figure 11-b**), the overall strain levels (GMS and LMS, defined across skin layers) measured in cases B are lower than those obtained for cases A. This would suggest that that the structural and mechanical effects of a soft viable epidermis (E_{VE} = 0.05 MPa) are a reduction in the strain levels across skin layers.

3.6 Global and local strains in the *stratum corneum* for the extension case

In simulated extension, for case A, maximum tensile strains (maximum principal strains) are observed for the soft *stratum corneum* (cases A1 and A3) in the superficial furrow zone F with LMS of 36% (9.6% GMS) and the shallow furrow zone D with LMS of 17.8% (4.75% GMS). Theses strain magnitudes are significantly higher than in the other zones (**Figure 12-a**). Zone G experiences a 0.2% LMS. For a stiffer *stratum corneum*, differences in LMS between anatomical zones are less pronounced (**Figure 12-b**). Zone F still experiences maximum strain levels, closely followed by zones K, H and D. Naturally, the GMS values are much smaller (0.76% compared to the soft *stratum corneum* case of 3.76%).

For all cases (E_{SC} = 0.6 MPa and E_{SC} = 370 MPa, cases A and B, **Figure 12**, **Figure 13**), higher tensile LMS is produced in the furrow zone compared to the surrounding crests (e.g. LMS for furrow B is 71% while crest A and C show LMS of 33% and 48%, respectively, **Figure 12**-b).

For cases B and low stiffness of the *stratum corneum* (cases B1 and B3), furrow zones D, F and H exhibit the highest LMS values (LMS=13.6%; 2.5% GMS) while the lowest LMS are found in zone G (LMS 2.16%; 0.39% GMS) (**Figure 13-a**). When the Young's modulus of the *stratum corneum* is increased from 0.6 MPa to 370 MPa, (cases B2 and B4), higher LMS values are found in case B4 at furrow zones F, H and K, with maximum values in zone F with LMS of 1.44% (2.93% GMS) and zones H and K with LMS of 1.01% (2.07% GMS) (**Figure 13-b**). If Poisson's ratio of the *stratum corneum* is reduced from 0.45 to 0.3 (case B2), strain levels in zones F are reduced to 1.08% LMS (2.66% GMS) and zones H and K to 0.84% LMS (2.08% GMS). All of the crests show similar values of LMS ranging from 0.36% to 0.53% (0.48 to 1.10% GMS) for case B4 and from 0.26% to 0.46% (0.65 to 1.14% GMS) for case B2.

For both cases A and B, variations in the Poisson's ratio of the *stratum corneum* did not lead to significant differences in the GMS of the whole skin model under extension.

3.7 Influence of the viable epidermis stiffness on the strain magnitude in the *stratum corneum*

To assess the sensitivity of the principal strains in the *stratum corneum* to the mechanical properties of the viable epidermis at each of the characteristic topographic locations (**Figure 5**), box plots of the minimum and maximum principal strains were used for the case of compression (**Figure 14** and **Figure 15**) and extension (**Figure 16** and **Figure 17**), respectively, for each value of the Young's modulus of the viable epidermis (case A, E_{VE} = 0.6 MPa; case B, E_{VE} = 0.05 MPa). For each zone, the principal strains of each finite element of the *stratum corneum* layer were evaluated at the centroid of the element and accounted for in the distribution evaluation. Each particular zone's response is described in terms of the median value (50th percentile of the distribution), the statistical dispersion defined by the interquartile range (IQR) (*i.e.* range of values between the first (25%) and third quartiles (75%)) and the peak values range (PVR) (range between the minimum and maximum values).

Within data sets, data points located in the tail of the distribution curves are classified as **near** or **far outliers** according to the following criteria (Wolfram Research, 2014):

$$Q_1 + 1.5(\text{IQR}) < \text{near outlier} < Q_1 - 1.5(\text{IQR}); \quad Q_3 + 3(\text{IQR}) < \text{far outlier} < Q_1 - 3(\text{IQR}) \tag{3}$$

Here Q_1 and Q_3 are respectively the first (25^{th} percentile) and third (75^{th} percentile) quartiles of the distribution. Although still accounted for in the PVR, the outliers are ignored in the figures for better visualisation. The range bars indicate values of the extreme data points that are not classified as outliers.
The deformed geometry of the *stratum corneum* was nearly identical in both cases A (where viable epidermis and dermis feature the same material properties) and B (where the three layers' properties are distinct) when subjected to compressive or extensive deformation (**Figure 6**-**Figure 9**). However, when considering the strain magnitude in the *stratum corneum* a different picture emerges.

Under skin compression, median values for the minimum principal strains in the *stratum corneum* can reach 19.2 % (case A1, **Figure 14**) and 6.8 % (case B1, **Figure 14**) depending on the anatomical locations, showing lower dispersion levels for case B1. Increasing the Young's modulus of the *stratum corneum* from 0.6 to 370 MPa (**Figure 15**, cases A2 and B2) has a drastic effect on the median and peak values of the minimum principal strains which are reduced in amplitude and exhibit lower variations across the anatomical zones considered. These median values do not exceed 1 %.

For the case of skin extension, there is a wide distribution of maximum principal strain values reaching up to 50 % in the interquartile range (**Figure 16**, cases A1 and B1) with a very heterogeneous response when considering each anatomical zone. The median values are predominantly lower in case A1, while the amplitude of dispersion is substantially reduced in case B1. For a stiffer *stratum corneum* (E_{SC} = 370 MPa), the maximum principal strain ranges in the *stratum corneum* are significantly reduced (**Figure 17**). Median values lie within the 0-1.5% range. Lower median strains and dispersion levels are observed in case B2.

It was found that the principal strain PVR representing the maximum dispersion was correlated to the geometry at the furrow. This was established by conducting a regression analysis (**Figure 21**) using a logarithmic form $f(d) = m \cdot \ln(d) + b$, where $f(x) = \text{PVR}$ and d is the furrow depth. **Table 3** lists the parameters m and b of the regression function corresponding to each of the tests and their respective coefficient of determination, R^2. The coefficients of determination between the simulation results and the values estimated by the logarithmic regression were $R^2 > 0.69$ for compression and $R^2 > 0.81$ for extension.

Under macroscopic compressive load the *stratum corneum* exhibits the following mechanical response at the characteristic anatomical locations:

- **Crests (A, C, E, G, J, L):** The LMS lie in the same respective range for each specific case (A1, A2, B1, B2) with average minimum principal strains from -0.08 % to -3.37 % when the Young's modulus of the *stratum corneum* is minimal (**Figure 14**) and do not exceed -0.35 % when it is maximal (**Figure 15**). Lower dispersion levels (IQR) are observed in the more protruding crests.
- **Deep furrows (B, H):** The intensity of the LMS is significantly reduced by the presence of a soft viable epidermis and the stiffening of the *stratum corneum*, showing average minimum principal strain of -16.34 % and -6.02% for Cases A1 and B1 (**Figure 14**), and -0.43 % and -0.32 % for cases A2 and B2 (**Figure 14**). These values are significantly higher in magnitude than the ones observed for the crests. The IQR is similarly affected.
- **Superficial furrows (F, K):** The LMS is -11.37 % and -2.62 % minimum principal strain in cases A1 and B1, respectively (**Figure 14**), while it reduces to -0.64 % and -0.28 % for cases A2 and B2 (**Figure 15**). The dispersion levels are similar to the ones observed for the deep furrows.
- **Wide furrow (D)**: LMS values of minimum principal strain lie between those of the crests and deep furrows showing a reduction from -11.94 % to -5.97% for a soft *stratum corneum* (**Figure 14**), and from -0.58 % to -0.38 % for a stiff *stratum corneum* (**Figure 15**), due to the presence of a soft viable epidermis. The dispersion levels (IQR) in this area are similar to those observed in other furrows.

Higher LMS are observed in the shallower superficial furrow F for case A, shifting to the shallower deep furrow H for case B. The higher IQR dispersion values were found among furrows H and K (next to each other in terms of depth, but classified as deep and superficial, respectively). Correlation between principal strain PVR of all furrows and their respective depth are: for A1, R^2= 0.87; A2, R^2=0.86; B1, R^2=0.91; B2, R^2=0.69), showing higher overall dispersion in the deep furrows (**Table 3**).

Under macroscopic tensile load the *stratum corneum* exhibits the following mechanical response:

- **Crests (A, C, E, G, J, L):** The LMS lie in the same respective range for each specific case (A1, A2, B1, B2) with average maximum principal strains varying from 2.73 % (case A1) to 4.56 % (case B1) when the Young's modulus of the *stratum corneum* is minimal (**Figure 16**). When the Young's modulus of the *stratum corneum* is increased from 0.6 to 370 MPa these LMS are within 0.64 % and 0.36 % (**Figure 17**). Low dispersion levels (IQR) are observed in the more protruding crests (e.g. crests G and A had the lowest LMS for soft and stiff *stratum corneum*, respectively).
- **Deep furrows (B, H):** The intensity of the LMS is significantly amplified by the presence of a soft viable epidermis when the *stratum corneum* is soft, but this trend is reversed when the *stratum corneum* is much stiffer (E_{SC} = 370 MPa), showing average maximum principal strain of 4.55 % and 10.35 % for cases A1 and B1 (**Figure 16**), and -0.95 % and 0.68 % for cases A2 and B2 (**Figure 17**). These values are significantly higher in magnitude than the ones observed for the crests. The IQR are reduced by the presence of the soft viable epidermis, having a larger effect (i.e. more reduction) in the furrows showing larger dispersion in case A1. The opposite reaction is observed, at a lower scale, for a stiff *stratum corneum* (cases A2 and B2).
- **Superficial furrows (K):** The LMS is about 20.30 % and 10.98 % maximum principal strain in respectively cases A1 and B1 (**Figure 16**) while it goes down to 1.43% and 0.96% in cases A2 and B2 (**Figure 17**).The dispersion levels are similarly affected to the ones observed for the deep furrows, showing larger amplification due to the presence of the soft living epidermis and stiff *stratum corneum*.
- **Wide furrow (D)**: LMS values of minimal principal strain lie between those of the crests and deep furrows showing a reduction from 17.71 % to 13.67 % for a soft *stratum corneum* (**Figure 16**), and from 1.16 % to 0.47 % for a stiff *stratum corneum* (**Figure 17**), due to the presence of a soft viable epidermis. Dispersion levels (IQR) observed in furrow D are as low as the ones witnessed in the crests, unlike what is observed in compression.

Higher LMS are observed in the superficial furrows F and K, and in the shallower deep ridge H. The higher IQR dispersion values were found mainly at deep furrow H. Correlation between principal strain PVR of all furrows and their respective depth are: for A1, R^2= 0.81; A2, R^2=0.91; B1, R^2=0.85; B2, R^2=0.91), showing higher overall dispersion in the deep furrows (**Table 3**).

Generally, **Figure 14**-**Figure** 17 show that, for the **compression** case, the LMS and IQR of principal strain magnitude and directions in the *stratum corneum* can be significantly affected by the value of the Young's modulus chosen for the viable epidermis provided that the Young's modulus of the *stratum corneum* is approximately an order magnitude greater. These effects are more or less pronounced depending on the topographical features of the *stratum corneum* (zones A-L). When considering the **extension** case, significant difference exists between the case of E_{VE} = 0.6 MPa and E_{VE} = 0.05 MPa (cases A and B). There appears to be much more significant change in LMS and IQR of strain in specific topographic zones compared to the compression case. Moreover, for the case when E_{SC} = 370 MPa (cases A2 and B2), lowering the Young's modulus of the viable epidermis from 0.6 to 0.05 MPa has the effect of reversing the direction of principal strains in some of the features.

The effect caused by the presence of a lower stiffness viable epidermis is a major result to consider in the light of all multi-layer finite element models of the skin found in the literature which typically assume flat interface between layers. These models are unlikely to capture these effects even by varying the Young's modulus of the viable epidermis.

3.8 The role of structural features of the skin and *stratum corneum* stiffness in strain reduction/amplification

One of the key objectives of this study was to assess the level of strain in the *stratum corneum* during simulated in-plane compression and extension of the skin. An important aspect to consider concerns the possible variations of the *stratum corneum* stiffness as a function of environmental or ageing conditions which, in turn, are likely to affect strain magnitude in the *stratum corneum*. To assess the effect of variations of the Young's modulus of the *stratum corneum* and also that of the viable epidermis a strain ratio metric was defined.

The strain ratio metric R was defined as the ratio of principal strains (i.e. minimum and maximum principal strains respectively for compression and extension) of the compared model (models A2, B2, E_{SC} = 370 MPa) over those of the reference model (models A1, B1, E_{SC} = 0.6 MPa) at each of the elements composing the skin model. R = 1 indicates that strain levels remain the same, R > 1 indicates an amplification of strains, 0 < R < 1 a reduction in the strain levels. A negative value for R implies a change in the principal direction of strain (from compressive to tensile and *vice versa*). Distribution of ratios of principal strains in the compression and extension cases are respectively depicted in **Figure 18** and **Figure 19** for models A1, A2, B1 and B2 and described in the following section. For each of the topographical zones, the median value of the strain ratio metric distribution R_m is taken to represent the ratio of amplification or reduction while the IQR for these distributions is a measure of dispersion.

3.8.1 Compression

As intuitively expected, increasing the Young's modulus from E_{SC} = 0.6 MPa to E_{SC} = 370 MPa significantly reduces the principal strains in the *stratum corneum* (**Figure 18**) for all characteristic anatomical zones, with a GMS ratio (i.e. the median ratio observed for the whole *stratum corneum* elements) of $R \approx 0.1$. The minimum principal strains are mostly reduced in deep furrows with an average median value of $R \leq 0.05$ for both cases A and B. The wide furrow D and the shallower superficial furrow F follow close with $R < 0.06$ and $R < 0.075$ for cases A and B, respectively. With respect to dispersion, most of the furrows show a rather homogeneous reduction of strains with IQR <0.075 except for furrow K (IQR ≤ 0.50).
Minimum reduction is found in crest L as R is 0.45 for both cases. The most remarkable result is shown in the most protruding crest G, as while R = 0.15 with a dispersion ratio of 0.21 is found in case A, the resulting ratios for case B shows an amplification of R = 1.57 and IQR of 3.37. These results show how heterogeneous the effect is in the elements contained in this crest. In general, greater R values are observed in the crests, and lower ones in the furrows.

3.8.2 Extension

Like in the load case corresponding to in-plane compression of the skin, stiffening of the *stratum corneum* by a factor in excess of a 600 induces a significant reduction in the magnitude of principal strains (**Figure 19**) with a GMS ratio R < 0.20. However, unlike the case of compression where the GMS ratio was similar between cases A and B, the GMS ratio of case A is larger than the one observed in case B by a factor of about 2. Regardless of that, both cases show particularly different behaviours in terms of the reduction and amplification of strains in each of the topographic features. For case A, the maximum principal strains are mostly reduced in the shallower furrows (R < 0.08), but a relevant contrast between the two superficial and the two deep furrows is observed (i.e. a 3 to 5 times larger ratio is observed in the deeper furrow of each category). The ratio in most of the crests ranges from 0.12 to 0.44 with no shape dependency. In contrast, crest G, exhibits a significant amplification factor (R = 2.20).
For case B, the distribution of R is rather homogeneous across the topographic features, with a range between 0.05 and 0.16 for crests and between 0.04 and 0.11 for furrows. Although a lower ratio is observed in the wide furrow D and a larger ratio at the crest G, no topographic shape dependency is observed.

3.9 Influence of the skin topography on the distribution and modulation of strains across skin layers

In **Figure 22** and **Figure 23** the ratio of the strain distribution magnitude of each skin layer (*stratum corneum*, viable epidermis and dermis) over the respective applied macroscopic strain (20%) is reported for each case A1, A2, B1 and B2. This metric expressed in % assess whether the magnitude of applied macroscopic strain is amplified or reduced in the skin layers. A value above or below 100 % means that strains are respectively magnified or reduced. This effectively highlights the effect of the structural properties of the skin layers in redistributing strains—and so the stress—within the skin.
Even when the skin is modelled as a homogeneous material (case A1) the median proportional strain values of the outer layer are remarkably lower than the ones observed in the layers underneath. For case A, it is observed that strains in the dermal layer are the least attenuated whilst those in the *stratum corneum* experience the largest reduction. For case B, strains in the viable epidermis are the least attenuated. When the Young's modulus of the *stratum corneum* is increased from 0.6 to 370 MPa, the magnitude of strain is obviously reduced and so is the dispersion.

In **compression** (**Figure 22**), the proportional median strain levels in cases A and B are respectively 7 and 15 times lower for the stiffer *stratum corneum*, while the dispersion levels are reduced 20 and 12 times for the IQR, and 6 and 9 times for the PVR. The changes in the stiffness of the *stratum corneum* have a marginal effect in the proportion of macroscopic strains transmitted to the viable epidermis and dermis. Between cases A1-A2 and B1-B2, the median values of this proportion are hardly altered in the dermis.

For **extension** (**Figure 23**), the change in stiffness of the *stratum corneum* has a relatively different effect as the median proportional strain levels in cases A and B are respectively 5 and 13 times lower as the Young's modulus of this layer increases, while the dispersion levels are reduced 9 and 11 times for the IQR, and 25 and 10 times for the PVR. The stiffening of the *stratum corneum* not only increases the median values of the proportional maximum principal strain distributions in the layers underneath, but also has an important effect on their dispersion parameters. The increase of proportional strain in the viable epidermis is 20% and 40% for cases A and B respectively, and 25% and 4% for the dermis. The interquartile dispersion is augmented on average by 50% for the viable epidermis in both cases, but for the dermis the IQR doubles in case A, while a negligible reduction is observed for case B. In terms of peak values dispersion, the results show negligible variation for the dermis and case A for the viable epidermis, while the PVR of case B2 is 2.5 times larger than the one observed in case B1.

4 Discussion

The imaged-based computational study presented in this paper has highlighted and quantified the critical role of the structural and mechanical characteristics of the skin layers over their mechanical response under tension and compression as well as on the global response of the skin as a 2D composite structure. Given that the skin is the human body's interface to the external environment, these results have implications for a variety of mechanical and/or mechanobiological processes (Limbert and Simms, 2013) across many domains of application including skin tribology in general (van Kuilenburg et al., 2013a, b; Veijgen et al., 2013b), pressure sores (Brand, 2006) and wound healing (Evans et al., 2013).

Geerligs (2010) stated that, during stretching of the skin, the *stratum corneum* partially unfolds without elongating, but to the best of our knowledge, this had not been previously quantified until now. In our 2D study it was revealed that, for a given imposed in-plane macroscopic deformation of the skin and fixed value of Young's modulus of the *stratum corneum*, the magnitude of strain in the *stratum corneum* tends to be significantly attenuated, particularly at specific topographic locations (crests, see **Figure 5** and **Figure 10**-**Figure 13**). When all layers have identical mechanical properties (case A1), this phenomenon is still present. There is, therefore, evidence that the convoluted geometry of the *stratum corneum*, in its own, is a contributor to this effect. When each skin layer features different mechanical properties, in addition to the stratum corneum, the contribution of the viable epidermis and dermis to these structural effects is modulated by the balance of mechanical properties between these three layers. When the viable epidermis is 12 times softer than the dermis this strain reduction effect in the *stratum corneum* is even stronger (cases B1-B4). In all the cases considered in the computational analyses, the strain deflection mechanism provided by the topographical features of the *stratum corneum* and underlying layers is clear. In all cases the 75th percentile of the *stratum corneum*'s finite elements experience a strain lower than half of the applied macroscopic strain. Similarly, in most of the results, more than 75% of the finite elements contained in the deeper layers sustain less than the total applied macroscopic strain. For case B, results show that the viable epidermis is the most strained layer, experiencing 2.5 to 3 times more strain than those that are macroscopically applied.

It was shown that the stiffness of the *stratum corneum* plays a critical role in conditioning the folding characteristics of the skin surface in both simulated in-plane (parallel to the outer surface of the skin) compression and extension of the skin (**Figure 6**-**Figure 9**). When the *stratum corneum* tends to stiffen—for example, as a result of a dryer external environment—cavities are likely to form in deep furrows, between skin folds, in compression while, in extension, the bottom surface of furrows experience limited rotation and significant strains. In this latter case, the base of a deep furrow acts like the fixed axis of a hinge mechanism in which the surrounding "vertical walls" of the furrow undergo large rotations with minimal straining. This observation suggests that, for the simulated 2D loading conditions, deep furrows convert in-plane deformations into out-of-plane deformations. In compression, this is very similar to the buckling of a column where compressive loads are converted into bending loads. Moreover, this functionality creates concentrated high strain zones in the deeper layers of the epidermis and dermis. Interestingly, dermal papillae tend to be very small or non-existent immediately under deep furrows and there might be a causal correlation here which could be relevant to the mechanobiology of skin.

The surface topography of the skin and how it deforms under loads are critical factors to consider for applications where the skin undergoes contact interactions with external devices like consumer good products (e.g. for dry and wet shaving the skin interacts with metal and polymer components, water, body secretions, gel or foam) or cosmetic agents (e.g. moisturiser). The aforementioned strain reduction and amplification mechanisms are therefore potentially very important to consider. Depending on the initial stiffness of the *stratum corneum* and its structural geometry, the skin will produce certain types of mechanical response, particularly if one considers the presence of a liquid thin-film (e.g. shave preparation) which introduces additional complex tribophysical phenomena (Israelachvili, 2011; Pailler-Mattei et al., 2007; Pailler-Mattei et al., 2006; Pailler-Mattei and Zahouani, 2004). The application of water-based agents to the skin has a plasticising effect on the *stratum corneum* which drastically reduces its Young's modulus (Wu et al., 2002, 2006). In these conditions, where friction forces tend to increase, rubbing of hard or softer surfaces against the skin can generate significant local strains which, in turn, can lead to important strain and stress redistribution in the underlying skin layers. The 2D computational study presented in this paper demonstrated the complex interplay between the material and structural properties of the skin layers during simulated compression and extension of the skin and therefore highlighted the importance of faithfully capturing these characteristics for reliable numerical analyses, especially when they are used to assist design decisions in industrial applications.

The numerical analyses showed that, for a given imposed macroscopic deformation of the skin, increasing the Young's modulus of the *stratum corneum* from 0.6 to 370 MPa led to higher strains in the deeper layers of the skin (viable epidermis and dermis). Drying stresses arising as a result of water loss in the *stratum corneum* (Levi et al., 2010) are generally perceived through the feeling of skin "tightness". Given that the *stratum corneum* has no mechanoreceptors capable of sensing changes in the homeostatic state of stress and/or strain, the computational results are consistent with this observation, namely that stiffening of the *stratum corneum* in combination with in-plane loads increases the depth of influence of mechanical stress/strain which reaches deeper in the viable epidermis and dermis where free nerve endings, Merkel cells, Meissner's, Ruffini's and Pacinian corpuscules are located (Shimizu, 2007).

As in any computational model, a number of limiting assumptions had to be made. The major limitation of the present model concerns its restriction to 2D geometry, boundary and loading conditions. The computational model was restricted to 2D due to the imaging technique used in this study and a desire to focus on the simplest modelling approach that would facilitate interpretation of results. An extension to 3D, straightforward in principle, would likely affect the results. However, based on the 2D results, one would also expect a strong influence of the structural and material properties of each skin layer on strain/stress magnitude and distribution as well as on surface topography. The 2D model is already a significant addition to what has been proposed in the literature so far. To the best of the authors' s knowledge, the proposed micromechanical model is the first to account for such a level of structural details for the skin (high-fidelity anatomical geometries for the *stratum corneum*, living epidermis and papillary dermis) and the objectives were to assess how such structural features play a role in transforming macroscopic strains and redistribute loads. The emphasis was on identifying structural effects on a 2D model and use that to suggest potential deformation mechanisms occurring in real skin structures. The simulations highlighted potentially important effects that are missed by idealised multi-layer models of the skin. The present study is a first attempt to pave the way for more advanced 3D microstructural models of the skin. The complex 3D patterns of sulci and how they might control deformations of the upper part of the epidermis should be explored in future studies.

The constitutive models used for the skin layers were based on isotropic neo-Hookean elasticity and ignored viscoelasticity. There is evidence that the *stratum corneum* possesses anisotropic properties (Geerligs, Oomens, et al., 2011). Due to its high content of collagenous fibres, the dermis also has directional properties. Thanks to the work of the Austrian anatomist Karl Langer (Langer, 1861, 1978a, b) it has been known since the 19th century that the skin is in a state of residual tension *in vivo*. Flynn et al. (2013a; 2013b) determined a relation between the *in vivo* the relaxed skin tension lines (RSTL) on a human face and the directional dependency of the skin stiffness using a combination of contact measurement techniques and inverse finite element methods. These authors demonstrated the need to account for these tension lines in the characterisation of the anisotropic properties of the human skin. It is noteworthy that mechanical anisotropy of the skin is due to the combined effects of the presence of Langer lines and to the anisotropy induced by the structural characteristics of the skin layers and their sub-structural components. In-plane anisotropy of the skin is correlated with Langer lines (Ní Annaidh et al. (2011) while out-of-plane (or across-the-thickness) anisotropy is due to the distinct mechanical properties and complex 3D structure of the skin layers. In the dermis, the organisation of collagen changes from loose and tortuous fibres in the papillary dermis to large dense stratified fibre bundles in the reticular dermis (Shimizu, 2007). The inclusion of such features (residual strains and fibrous microstructure) in a microstructural finite element model of the skin, although possible in principle, would only make sense in a 3D setting and would require significantly more information on skin microstructure, data on the level and 3D directions of pre-strain in the specific skin sample (*i.e.* consistent with anatomical location) and may likely require higher resolution imaging modalities. In a 3D finite element context, the question of reliably applying pre-strains with regards their non-uniform distributions and directions would present technical challenges (Limbert et al., 2004; Rausch and Kuhl, 2013; Weiss et al., 1995). The aforementioned observations provide justification to the choice of using initially stress-free 2D computational multi-layer skin models.

The composite skin model did not account for the full thickness of the dermis and its underlying hypodermis. Addressing this limitation would likely affect the results by reducing the effect of imposed boundary conditions, particularly the symmetry boundary. Future computational analyses should also include skin appendices such as hair follicles and pores which could play a mechanical role in redistributing strain and stress in the skin as well as in stopping fracture propagation in the (drying) *stratum corneum*.

All skin layers were assumed to be perfectly bonded to each other without the presence of any intermediary interface. This simplifying assumption was deemed necessary to focus on other factors, namely, the geometrical and material properties of each layer. It was also necessary due to the significantly higher computing power that this would have required because of the level of mesh refinement needed. The living epidermis is connected to the underlying dermis through a 3D interlocking wavy interface called the dermal-epidermal junction (DEJ) or *basal lamina* which is effectively a 0.5-1 μm thick basement membrane (Chan, 1997).

In the epidermis, the basal cells of the *stratum basale* are connected to the basement membrane by anchoring filaments of hemidesmosomes while the cells of the papillary dermis connect to the basement membrane through type VII collagen fibrils. The geometry and material properties of these structural elements are likely to play a critical role in load transmission between layers, particularly in 3D. Future studies should investigate this further but are likely to require a multiscale approach given the large span of spatial dimensions involved.

As is always the case with mathematical and computational models, a critical step, before relying on the predictive capabilities of these models, is to validate them—even partially—using physical experiments. This is currently very challenging but there are very promising emerging approaches in skin research. For example, using digital image correlation techniques it is possible to obtain full (strain) field measurements (Tonge et al., 2013a; Tonge et al., 2013b). The modelling approach adopted here is a first step towards models to assess, understand and control the effects of the structural properties of skin in medicine, biology and industrial applications.

In the last few years, the concept of skin microclimate has been in the spotlight with regards to pressure ulcer research (Gefen, 2011). Skin microclimate encompasses a number of physical factors such as temperature, humidity and air flow at the skin surface. These interacting factors are believed to play a critical role in compromising skin integrity by reducing its natural barrier function. These effects are amplified when the skin acts as a load-bearing surface, particularly when subjected to shear loads (Zhong et al., 2006). There is evidence that the skin surface topography changes during loading but it is unclear whether these changes are purely driven by mechanics or partly induced by microclimate factors such as temperature and moisture (Kottner et al., 2013; Veijgen et al., 2013a). The models developed in our study offer the potential to address these questions by either focusing on the mechanics only or by considering coupled thermo-mechanical effects combined with moisture absorption or exudation. Our study showed that, during in-plane compression of the skin, if the Young's modulus of the *stratum corneum* and the viable epidermis are both 0.6 MPa (low end of the spectrum for the *stratum corneum*) maximum strains are located in the dermis and lower regions of the viable epidermis rather than branching from the skin surface (**Figure 6**). When considering the viable epidermis with a Young's modulus 12 times lower, strains are intensified in these regions (**Figure 7**). This effect increases the likelihood of compromising the integrity of the dermal-epidermal junction (DEJ) which is believed to play a major role in the chemo-mechano-biology of the skin. Indeed, the DEJ controls the transit of molecules between the dermis and epidermis according to their dimension and charge. It allows the passage of migrating and invading cells under normal (i.e. melanocytes and Langerhans cells) or pathological (i.e. lymphocytes and tumour cells) conditions (Burgeson and Christiano, 1997). However, it is important to reiterate that the results were obtained for a 2D setting and, that future 3D studies may unravel more complex structural effects.

After an injury, the folding/unfolding or straining of the skin furrows may play an important role during the scar formation process by controlling the mechanical environment around a wound (Wong et al., 2012). This environment has been clinically shown to be of the utmost importance for conditioning scar tissue formation (Longaker et al., 2011). Using an external device to mechanically shield a wound, Longaker et al. (2011) showed that creating a mechanical equilibrium state around the wound would in turn lead to homeostasis (biological equilibrium), effectively inhibiting the production of new scar tissue with undesirable structural and mechanical characteristics (e.g. fibrosis). There is evidence that mechanical tension can induce phenotypic alteration in fibroblasts during wound healing under the form of altered collagen network characteristics (Dunn et al., 1985). These effects lead to hypertrophic scar tissue formation where the new tissue features a reduced extensibility rather than an increased stiffness. Compared to normal skin, scar tissue loses the uncrimping phase of the typical *J*-shape of the tensile stress-strain curve (Fung, 1981). Recently, using a 3D *in vitro* tissue engineered model, Suarez et al. (2014) demonstrated that skin tension up-regulates tension-related gene expression in keloid fibroblasts thus confirming the role of mechanics as a regulator of the scarring process.

There have been few computational studies in the literature examining the mechanical or chemo-bio-mechanical environment around a wound or skin suture. In a recent computational study examining the mechanics of local skin flaps after tissue expansion, Tepole et al. (2014b) suggested a direct correlation between regions of maximum stress and tissue necrosis. Their model considered the skin as a mono-layer transversely isotropic hyperelastic structure. Cerda (2005) developed a mechanical model of wound contraction in skin with special focus on wrinkles induced by the existence of residual tension in the skin. To analyse stress and displacement distributions produced by different wound shapes and suture patterns, (Chaudhry et al., 1998) established a 2D mathematical model of the skin. Skin was assumed to be a linear orthotropic elastic material. Following a similar motivation, Flynn (2010) developed a series of finite element models featuring different types of wound shapes and compared the distribution and magnitude of stress. The skin was modelled as an orthotropic hyperelastic material (Bischoff et al., 2002).

In all these numerical studies the skin was assumed to be either a 2D or 3D homogeneous structure. There was no account of realistic anatomical skin topography or geometry of the *stratum corneum*, living epidermis and dermis.

It is often assumed that the collagen-rich dermis is the main mechanical contributor to the macroscopic response of the skin, particularly under finite extension. However, under surface loads or loads applied in the upper strata of the skin like in the present study, there is a complex mechanical interplay between these layers. If one considers these purely mechanical phenomena in combination with the presence of a wound it is straightforward to anticipate that the coupled mechanobiological processes involved in epidermal and dermal wound healing (Vodovotz et al., 2008) would be affected by the microstructural response of the skin. In the light of the computational results obtained in the present study, it is suggested that past computational studies should be revisited by incorporating anatomical geometries into skin models, ideally in 3D, in order to provide additional insight.

5 Conclusion

The study presented in this paper has introduced a 2D image-based finite element modelling approach, with special emphasis on anatomical realism, to study the microstructural and mechanical interplay of the *stratum corneum*, viable epidermis and dermis layers of the human skin under simulated in-plane compression and extension. The hybrid experimental-computational methodology has proven to be robust and has offered valuable insights into the simulated 2D mechanics of the skin, and that of the *stratum corneum* in particular, by providing qualitative and quantitative information on strain magnitude and distribution. The implications of this study are many-fold across a wide range of sectors where simulating the mechanics of the skin is relevant, particularly in biomedical, consumer goods, cosmetics, sport equipment and computer graphics. Based on 2D finite element simulations, it appears that the geometry of the skin layers (together with their material properties) could play a significant role in controlling the local mechanical environment at the surface and within the skin.

The series of finite element analyses has highlighted and quantified the following key points

- Through a complex non-linear interplay, the geometry and mechanical characteristics of the skin layers (and their relative balance), play a critical role in conditioning the 2D skin mechanical response to macroscopic in-plane compression and extension. Topographical features of the skin surface such as furrows were shown to offer an effective means to deflect, convert and redistribute strain—and so stress—within the *stratum corneum*, viable epidermis and dermis. This is achieved through geometrical features and structural effects that energetically favour certain deformation modes like bending. A corollary consequence of these phenomena is that strains can be amplified or reduced in certain locations of the skin structure. This confirms the work hypothesis of the present study although these conclusions are based on a 2D approach and it is therefore important to exercise caution in the interpretation of the results, particularly with regards to the real 3D characteristics of the human skin (e.g. material and structural properties as well as residual tension lines). Extension of the model to 3D is likely to highlight comparable structural effects in terms of deformation mechanisms (i.e. local modulation of macroscopic strains) but potentially different in terms of spatial distributions and orientations. Future studies should investigate these questions.
- Despite the small thickness of the *stratum corneum*, its Young's modulus has a significant effect not only on the magnitude and directions of the strains it experiences but also on those of the underlying layers. This effect is reflected in the deformed shape of the 2D skin surface in simulated compression and extension and is intrinsically linked to the rather complex geometrical characteristics of each skin layer. Moreover, if the Young's modulus of the viable epidermis is assumed to be reduced by a factor 12, the area of skin folding is likely to increase under skin compression. These results should be considered in the light of published computational models of the skin which, up to now, have ignored these characteristics.
- Stiffening of the *stratum corneum*, for example, as a result of a dryer environment, has consequences not only for its own mechanical response but also for the underlying viable epidermis and dermis because of the intimate mutual structural relations between these layers.

Acknowledgments

Maria-Fabiola Leyva-Mendivil is partially supported by a CONACyT scholarship. Georges Limbert was partially supported by the Engineering and Physical Sciences Research Council [EP/F034296/1]. The authors would like to acknowledge the financial support of these organisations and thank Dr. David-John O'Callaghan of Procter & Gamble for many fruitful discussions.

6 References

Alexiades-Armenakas, M., 2007. Fractional laser resurfacing, J Drugs Dermatol 6, 750-751.

Areias, P.A., Jorge, R.M.N., Barbosa, J.T., Fernandes, A.A., Mascarenhas, T., Oliveira, M., Patricio, B., 2003. Experimental and finite element analysis of human skin elasticity, 2003 Advances in Bioengineering, 303-304.

Batisse, D., Bazin, R., Baldeweck, T., Querleux, B., Levêque, J.L., 2002. Influence of age on the wrinkling capacities of skin, Skin Res Technol 8, 148-154.

Bellemere, G., Stamatas, G.N., Bruere, V., Bertin, C., Issachar, N., Oddos, T., 2009. Antiaging action of retinol: from molecular to clinical, Skin Pharmacology and Physiology 22, 200-209.

Belytschko, T., Liu, W.K., Moran, B., 2000. Nonlinear Finite Elements for Continua and Structures. Wiley, Oxford.

Bhushan, B., 2012. Nanotribological and nanomechanical properties of skin with and without cream treatment using atomic force microscopy and nanoindentation, Journal of Colloid and Interface Science 367, 1-33.

Bischoff, J.E., Arruda, E.M., Grosh, K., 2000. Finite element modeling of human skin using an isotropic, nonlinear elastic constitutive model, J Biomech 33, 645-652.

Bischoff, J.E., Arruda, E.M., Grosh, K., 2002. Finite element simulations of orthotropic hyperelasticity, Finite Elem. Anal. Des. 38, 983-998.

Boissieux, L., Kiss, G., Thalmann, N.M., Kalra, P., 2000. Simulation of skin aging and wrinkles with cosmetics insight, Computer Animation and Simulation 2000, 15-27.

Bolognia, J.L., Braverman, I.M., Rousseau, M.E., Sarrel, P.M., 1989. Skin changes in menopause, Maturitas 11, 295-304.

Brand, P.W., 2006. Pressure sore--the problem, J Tissue Viability 16, 9-11.

Buganza Tepole, A., Kuhl, E., 2014. Computational modeling of chemo-bio-mechanical coupling: a systems-biology approach toward wound healing, Comput Meth Biomech Biomed Eng, 1-18.

Burgeson, R.E., Christiano, A.M., 1997. The dermal-epidermal junction, Current Opinion in Cell Biology 9, 651-658.

Cavicchi, A., Gambarotta, L., Massabo, R., 2009. Computational modeling of reconstructive surgery: The effects of the natural tension on skin wrinkling, Finite Elem. Anal. Des. 45, 519-529.

Cerda, E., 2005. Mechanics of scars, J Biomech 38, 1598-1603.

Chan, L.S., 1997. Human skin basement membrane in health and autoimmune diseases, Frontiers in Bioscience 2, 343-352.

Changizi, M., Weber, R., Kotecha, R., Palazzo, J., 2011. Are wet-induced wrinkled fingers primate rain treads?, Brain, Behavior and Evolution 77, 286-290.

Chaudhry, H.R., Bukiet, B., Siegel, M., Findley, T., Ritter, A.B., Guzelsu, N., 1998. Optimal patterns for suturing wounds, J Biomech 31, 653-662.

Dahlgren, R.M., 1984. Measurement of skin condition by sonic velocity, 19, 1-19.

Dauskardt, R.H., Levi, K., Kwan, A., Rhines, A.S., Gorcea, M., Moore, D.J., 2010. Emollient molecule effects on the drying stresses in human stratum corneum, Br J Derm 163, 695-703.

Dauskardt, R.H., Levi, K., Kwan, A., Rhines, A.S., Gorcea, M., Moore, D.J., 2011. Effect of glycerin on drying stresses in human stratum corneum, Journal of Dermatological Science 61, 129-131.

Dauskardt, R.H., Wu, K.S., van Osdol, W.W., 2006. Mechanical properties of human stratum corneum: Effects of temperature, hydration, and chemical treatment, Biomaterials 27, 785-795.

Delalleau, A., 2007. In vivo analysis of the skin mechanical properties, University Jean Monnet, Saint Etienne, France, PhD Thesis.

Delalleau, A., Josse, G., Lagarde, J.M., Zahouani, H., Bergheau, J.M., 2006. Characterization of the mechanical properties of skin by inverse analysis combined with the indentation test, J Biomech 39, 1603-1610.

Derler, S., Gerhardt, L.C., 2012. Tribology of Skin: Review and Analysis of Experimental Results for the Friction Coefficient of Human Skin, Trib Lett 45, 1-27.

Diridollou, S., Patat, F., Gens, F., Vaillant, L., Black, D., Lagarde, J.M., Gall, Y., Berson, M., 2000. In vivo model of the mechanical properties of the human skin under suction, Skin Res Technol 6, 214-221.

Duan, Z.Y., Tong, B.G., Jiang, G.Q., 2000. A finite-element formulation of heating rate and skin friction on the basis of conservation laws, Acta Mechanica Sinica 16, 128-132.

Dunn, M.G., Silver, F.H., Swann, D.A., 1985. Mechanical Analysis of Hypertrophic Scar Tissue: Structural Basis for Apparent Increased Rigidity, J Investig Dermatol 84, 9-13.

Elbischger, P.J., Bischof, H., Regitnig, P., Holzapfel, G.A., 2004. Automatic analysis of collagen fiber orientation in the outermost layer of human arteries, Pattern Analysis and Applications 7, 269-284.

Evans, N.D., Oreffo, R.O.C., Healy, E., Thurner, P.J., Man, Y.H., 2013. Epithelial mechanobiology, skin wound healing, and the stem cell niche, J Mech Behav Biomed Mater 28, 397-409.

Evans, S.L., 2009. On the implementation of a wrinkling, hyperelastic membrane model for skin and other materials, Comput Meth Biomech Biomed Eng 12, 319-332.

Flynn, C., 2010. Finite element models of wound closure, J Tissue Viability 19, 137-149.

Flynn, C., McCormack, B.A.O., 2008a. Finite element modelling of forearm skin wrinkling, Skin Res Technol 14, 261-269.

Flynn, C., McCormack, B.A.O., 2008b. A simplified model of scar contraction, J Biomech 41, 1582-1589.

Flynn, C., Stavness, I., Lloyd, J., Fels, S., 2013a. A finite element model of the face including an orthotropic skin model under in vivo tension, Computer Methods in Biomechanics & Biomedical Engineering.

Flynn, C., Taberner, A.J., Nielsen, P.M.F., Fels, S., 2013b. Simulating the three-dimensional deformation of in vivo facial skin, J Mech Behav Biomed Mater 28, 484-494.

Flynn, C.O., McCormack, B.A.O., 2009. A three-layer model of skin and its application in simulating wrinkling, Comput Meth Biomech Biomed Eng 12, 125-134.

Flynn, C.O., McCormack, B.A.O., 2010. Simulating the wrinkling and aging of skin with a multi-layer finite element model, J Biomech 43, 442-448.

Fung, Y.C., 1981. Biomechanics: mechanical properties of living tissues. Springer-Verlag, New York.

Geerligs, M., 2010. Skin layer mechanics, Department of Biomedical Engineering, TU Eindhoven, The Netherlands, PhD Thesis.

Geerligs, M., Oomens, C.W.J., Ackermans, P.A.J., Baaijens, F.P.T., Peters, G.W.M., 2011. Linear shear response of the upper skin layers, Biorheology In press.

Gefen, A., 2011. How do microclimate factors affect the risk for superficial pressure ulcers: A mathematical modeling study, J Tissue Viability 20, 81-88.

Groves, R.B., Coulman, S.A., Birchall, J.C., Evans, S.L., 2013. An anisotropic, hyperelastic model for skin: Experimental measurements, finite element modelling and identification of parameters for human and murine skin, J Mech Behav Biomed Mater 18, 167-180.

Gunner, C.W., Hutton, W.C., Burlin, T.E., 1979. The mechanical properties of skin in vivo—a portable hand-held extensometer, Br J Derm 100, 161-163.

Hendriks, F.M., Brokken, D., Oomens, C.W.J., Bader, D.L., Baaijens, F.P.T., 2006. The relative contributions of different skin layers to the mechanical behavior of human skin in vivo using suction experiments, Med Eng Phys 28, 259-266.

Hendriks, F.M., Brokken, D., van Eemeren, J., Oomens, C.W.J., Baaijens, F.P.T., Horsten, J., 2003. A numerical-experimental method to characterize the non-linear mechanical behaviour of human skin, Skin Res Technol 9, 274-283.

Holzapfel, G.A., Gasser, T.C., Ogden, R.W., 2000. A new constitutive framework for arterial wall mechanics and a comparative study of material models, J Elast 61, 1-48.

Israelachvili, J.N., 2011. Intermolecular and surface forces, Third edition ed. Academic Press, Burlington, MA, USA.

Jor, J.W.Y., Parker, M.D., Taberner, A.J., Nash, M.P., Nielsen, P.M.F., 2013. Computational and experimental characterization of skin mechanics: identifying current challenges and future directions, Wiley Interdisciplinary Reviews: Systems Biology and Medicine 5, 539-556.

Kareklas, K., Nettle, D., Smulders, T.V., 2013. Water-induced finger wrinkles improve handling of wet objects.

Kottner, J., Dobos, G., Blume-Peytavi, U., 2013. How does immobility affect the skin barrier?, 23rd Conference of the European Wound Management Association, Copenhagen, Denmark, p. 33.

Kuwazuru, O., Saothong, J., Yoshikawa, N., 2008. Mechanical approach to aging and wrinkling of human facial skin based on the multistage buckling theory, Med Eng Phys 30, 516-522.

Langer, K., 1861. Zur Anatomie und Physiologie der Haut. Über die Spaltbarkeit der Cutis, Sitzungsbericht der Mathematisch-naturwissenschaftlichen Classe der Wiener Kaiserlichen Academie der Wissenschaften Abt 44.

Langer, K., 1978a. On the anatomy and physiology of the skin: I. The cleavability of the cutis, British Journal of Plastic Surgery 31, 3-8.

Langer, K., 1978b. On the anatomy and physiology of the skin: II. Skin Tension (With 1 Figure), British Journal of Plastic Surgery 31, 93-106.

Lanir, Y., Dikstein, S., Hartzshtark, A., Manny, V., 1990. In-vivo indentation of human skin, J Biomech Eng 112, 63-69.

Larrabee, W.F., Galt, J.A., 1986a. A Finite-Element Model for the Design of Local Skin Flaps, Otolaryngologic Clinics of North America 19, 807-824.

Larrabee, W.F., Jr., 1986. A finite element model of skin deformation. I. Biomechanics of skin and soft tissue: a review, Laryngoscope 96, 399-405.

Larrabee, W.F., Jr., Galt, J.A., 1986b. A finite element model of skin deformation. III. The finite element model, Laryngoscope 96, 413-419.

Larrabee, W.F., Jr., Sutton, D., 1986. A finite element model of skin deformation. II. An experimental model of skin deformation, Laryngoscope 96, 406-412.

Lévêque, J.L., Audoly, B., 2013. Influence of Stratum Corneum on the entire skin mechanical properties, as predicted by a computational skin model, Skin Res Technol 19, 42-46.

Levi, K., Dauskardt, R.H., 2010. Application of substrate curvature method to differentiate drying stresses in topical coatings and human stratum corneum, International Journal of Cosmetic Science 32, 294-298.

Levi, K., Weber, R.J., Do, J.Q., Dauskardt, R.H., 2010. Drying stress and damage processes in human stratum corneum, International Journal of Cosmetic Science 32, 276-293.

Limbert, G., 2011. A mesostructurally-based anisotropic continuum model for biological soft tissues--Decoupled invariant formulation, J Mech Behav Biomed Mater 4, 1637-1657.

Limbert, G., 2014. Chapter 4: State-of-the-art constitutive models of skin biomechanics, in: Querleux, B. (Ed.), Computational Biophysics of the Skin. Pan Stanford Publishing Pte. Ltd, Singapore, pp. 95-131.

Limbert, G., Simms, C., 2013. Editorial: Special issue on skin mechanobiology, J Mech Behav Biomed Mater 28, 395-396.

Limbert, G., Taylor, M., 2002. On the constitutive modeling of biological soft connective tissues. A general theoretical framework and tensors of elasticity for strongly anisotropic fiber-reinforced composites at finite strain, Int J Solids Struct 39, 2343-2358.

Limbert, G., Taylor, M., Middleton, J., 2004. Three-dimensional finite element modelling of the human ACL: simulation of passive knee flexion with a stressed and stress-free ACL, J Biomech 37, 1723-1731.

Longaker, M.T., Gurtner, G.C., Dauskardt, R.H., Wong, V.W., Bhatt, K.A., Wu, K., Vial, I.N., Padois, K., Korman, J.M., 2011. Improving Cutaneous Scar Formation by Controlling the Mechanical Environment Large Animal and Phase I Studies, Annals of Surgery 254, 217-225.

Magnenat-Thalmann, N., Kalra, P., Leveque, J.L., Bazin, R., Batisse, D., Querleux, B., 2002. A computational skin model: fold and wrinkle formation, IEEE Trans Inf Technol Biomed 6, 317-323.

Marieb, E.N., Hoehn, K., 2010. Human Anatomy & Physiology, 8th edition ed. Pearson International Edition.

Matts, P., Hendrix, S., Barton, P., Vanoosthuyze, K., 2006. Stratum corneum protein and proinflammatory cytokine biomarkers as end points for understanding the effects of a high-efficacy body moisturizer containing niacinamide, J Am Acad Dermatol 54, Ab48-Ab48.

Ní Annaidh, A., Bruyère, K., Destrade, M., Gilchrist, M.D., Maurini, C., Otténio, M., Saccomandi, G., 2012. Automated estimation of collagen fibre dispersion in the dermis and its contribution to the anisotropic behaviour of skin, Ann Biomed Eng 40, 1666-1678.

Ní Annaidh, A., Bruyère, K., Destrade, M., Gilchrist, M.D., Otténio, M., 2011. Characterization of the anisotropic mechanical properties of excised human skin, J Mech Behav Biomed Mater 5, 139-148.

Ogden, R.W., 1984. Non-Linear Elastic Deformations. Ellis Horwood Ltd., West Sussex, England.

Pailler-Mattei, C., Pavan, S., Vargiolu, R., Pirot, F., Falson, F., Zahouani, H., 2007. Contribution of stratum corneum in determining bio-tribological properties of the human skin, Wear 263, 1038-1043.

Pailler-Mattei, C., Vargiolu, R., Zahouani, H., 2006. Analysis of adhesion contact of human skin in vivo, Contact Angle, Wettability and Adhesion, Vol 4, 501-514

529.

Pailler-Mattei, C., Zahouani, H., 2004. Study of adhesion forces and mechanical properties of human skin in vivo, J. Adhes. Sci. Technol. 18, 1739-1758.

Pannisset, F., Varchon, D., Agache, P., 1994. Non invasive measurement of stratum corneum Young's modulus in vivo.

Papir, Y.S., Hsu, K.H., Wildnauer, R.G., 1975. The mechanical properties of stratum corneum. I. The effect of water and ambient temperature on the tensile properties of newborn rat stratum corneum, Biochimica et Biophysica acta 399.

Park, A., 1972. Rheology of stratum corneum. I. A molecular interpretation of the stress-strain curve, J Soc Cosmet Chem 12.

Piérard, G.E., Uhoda, I., Piérard-Franchimont, C., 2004. From skin microrelief to wrinkles. An area ripe for investigation, J Cosm Derm 2, 21-28.

Raab, W.P., 1990. The skin surface and stratum corneum, Br J Dermatol 122 Suppl 35, 37-41.

Rausch, M.K., Kuhl, E., 2013. On the effect of prestrain and residual stress in thin biological membranes, J Mech Phys Solids 61, 1955-1969.

Serup, J., Jemec, G.B.E., Grove, G.L., 1995. Handbook of Non-Invasive Methods and the Skin, First edition ed. CRC Press, Boca Raton, FL, USA.

Shimizu, H., 2007. Shimizu's Textbook of Dermatology. Hokkaido University Press - Nakayama Shoten Publishers.

Suarez, E., Syed, F., Rasgado, T.A., Walmsley, A., Mandal, P., Bayat, A., 2014. Skin equivalent tensional force alters keloid fibroblast behavior and phenotype, Wound Repair and Regeneration 22, 557-568.

Tepole, A.B., Gart, M., Gosain, A.K., Kuhl, E., 2014a. Characterization of living skin using multi-view stereo and isogeometric analysis, Acta Biomater 10, 4822-4831.

Tepole, A.B., Gosain, A.K., Kuhl, E., 2014b. Computational modeling of skin: Using stress profiles as predictor for tissue necrosis in reconstructive surgery, Comput. Struct. 143, 32-39.

Tepole, A.B., Ploch, C.J., Wong, J., Gosain, A.K., Kuhl, E., 2011. Growing skin: A computational model for skin expansion in reconstructive surgery, J Mech Phys Solids 59, 2177-2190.

Tonge, T.K., Atlan, L.S., Voo, L.M., Nguyen, T.D., 2013a. Full-field bulge test for planar anisotropic tissues: Part I – Experimental methods applied to human skin tissue, Acta Biomater 9, 5913-5925.

Tonge, T.K., Voo, L.M., Nguyen, T.D., 2013b. Full-field bulge test for planar anisotropic tissues: Part II – A thin shell method for determining material parameters and comparison of two distributed fiber modeling approaches, Acta Biomater 9, 5926-5942.

Tran, H.V., Charleux, F., Ehrlacher, A., Ho Ba Tho, M.C., 2005. Propriétés mécaniques multicouches de la peau humain in vivo, modèle numérique anatomique, pp. 101-106.

van Kuilenburg, J., Masen, M.A., van der Heide, E., 2013a. Contact modelling of human skin: What value to use for the modulus of elasticity?, Proceedings of the Institution of Mechanical Engineers Part J-Journal of Engineering Tribology 227, 349-361.

van Kuilenburg, J., Masen, M.A., van der Heide, E., 2013b. The role of the skin microrelief in the contact behaviour of human skin: Contact between the human finger and regular surface textures, Tribology International 65, 81-90.

Veijgen, N.K., Masen, M.A., van der Heide, E., 2013a. Relating Friction on the Human Skin to the Hydration and Temperature of the Skin, Trib Lett 49, 251-262.

Veijgen, N.K., Masen, M.A., van der Heide, E., 2013b. Variables influencing the frictional behaviour of in vivo human skin, J Mech Behav Biomed Mater 28, 448-461.

Vodovotz, Y., Csete, M., Bartels, J., Chang, S., An, G., 2008. Translational Systems Biology of Inflammation, Plos Comput Biol 4, e1000014.

Waller, J.M., Maibach, H.I., 2005. Age and skin structure and function, a quantitative approach (I): blood flow, pH, thickness, and ultrasound echogenicity, Skin Res Technol 11, 221-235.

Waller, J.M., Maibach, H.I., 2006. Age and skin structure and function, a quantitative approach (II): protein, glycosaminoglycan, water, and lipid content and structure, Skin Res Technol 12, 145-154.

Wan Abas, W.A.B., 1994. Biaxial tension test of human skin in vivo, Biomed Mater Eng 4, 473-486.

Weiss, J.A., Maker, B.N., Govindjee, S., 1996. Finite element implementation of incompressible transversely isotropic hyperelasticity, Comput Meth Appl Mech Eng 135, 107-128.

Weiss, J.A., Maker, B.N., Schauer, D.A., 1995. Treatment of initial stress in hyperelastic finite element models of soft tissues, ASME Conference BED, pp. 105-106.

Wilhelm, K.P., Cua, A.B., Maibach, H.I., 1991. Skin aging. Effect on transepidermal water loss, stratum corneum hydration, skin surface pH, and casual sebum content, Arch Dermatol 127, 1806-1809.

Wolfram Research, I., 2014. Wolfram Mathematica 10.0 Manual. Wolfram Research, Inc.

Wong, V.W., Levi, K., Akaishi, S., Schultz, G., Dauskardt, R.H., 2012. Scar zones: region-specific differences in skin tension may determine incisional scar formation, Plastic and Reconstructive Surgery 129, 1272-1276.

Wu, K.S., Van Osdol, W.W., Dauskardt, R.H., 2002. Mechanical and microstructural properties of stratum corneum, Biological Biomimetic Materials-Properties to Function 724, 27-33.

Wu, K.S., van Osdol, W.W., Dauskardt, R.H., 2006. Mechanical properties of human stratum corneum: effects of temperature, hydration, and chemical treatment, Biomaterials 27, 785-795.

Zhong, W., Xing, M.M., Pan, N., Maibach, H.I., 2006. Textiles and human skin, microclimate, cutaneous reactions: an overview, Cutan Ocul Toxicol 25, 23-39.

Zöllner, A.M., Holland, M.A., Honda, K.S., Gosain, A.K., Kuhl, E., 2013. Growth on demand: Reviewing the mechanobiology of stretched skin, J Mech Behav Biomed Mater 28, 495-509.

Table 1: Linear elastic and corresponding neo-Hookean constitutive parameters for skin layers (SC - *stratum corneum*, VE - viable epidermis, D - dermis). Parameter values which were not in the original paper reference and that were derived for our study [e.g. calculation of neo-Hookean parameters from Young's modulus and Poisson's ratio and vice-versa, see equation (2)] are indicated in bold characters. The parameter D_1 is related to the bulk modulus κ_0 as $D_1 = 2 / \kappa_0$.

Layer	Linear elastic		Neo-Hookean		Test	Reference
	E (MPa)	ν	c_{10} (MPa)	D_1 (MPa^{-1})		
SC	0.60	0.3†	**0.115**	**4.000**	Human skin, *ex vivo* indentation	(Geerligs et al., 2011)
	1.20	0.3†	**0.231**	**2.000**	Human skin, *ex vivo* indentation	(Geerligs et al., 2011)
	6.00	0.50	**1.003**	**0.010**	FE model	(Magnenat-Thalmann et al., 2002)
	8.87	0.3†	**1.706**	**0.271**	Murine skin, tensile test	(Delalleau, 2007)‡[a]
	10.00	0.30	**1.923**	**0.240**	FE model	(Lévêque & Audoly, 2013) ‡[h]
	12.00	0.50	**2.007**	**0.005**	FE model	(Magnenat-Thalmann et al., 2002) §
	13.50	0.3†	**2.596**	**0.178**	Human skin, *ex vivo* out of plane test	(Wu, van Osdol, & Dauskardt, 2006)
	13.00	0.3†	**2.500**	**0.185**	Human skin, *in vivo*	(Delalleau, 2007)‡[b]
	57.80	0.3†	**11.115**	**0.042**	Human skin, *in vivo* sonic propagation	(Delalleau, 2007)‡[c]
	100.00	0.3†	**19.231**	**0.024**	Human skin, *in vivo* indentation	(Delalleau, 2007)‡[d]
	175.30	0.3†	**33.712**	**0.014**	Human skin, in-plane tensile test	(Wu et al., 2006)
	240.00	**0.48**	**40.535**	1010.000	Porcine skin, rheological test	(Flynn & McCormack, 2009) ‡[e]
	1000.00	0.3†	**192.308**	**0.002**	Human skin, *in vivo* indentation	(Delalleau, 2007)‡[d]
VE	**0.00**	0.3†	0.000	**4195.804**	Human skin, *in vivo* suction test	(Hendriks, Brokken, Oomens, Bader, & Baaijens, 2006)
	0.05	0.30	**0.010**	**48.000**	FE model	(Lévêque & Audoly, 2013) ‡[h]
	0.05	0.50	**0.008**	**1.200**	FE model	(Magnenat-Thalmann et al., 2002)
	0.05	0.50	**0.008**	**1.200**	FE model	(Magnenat-Thalmann et al., 2002) §
	0.60	0.3†	**0.115**	**4.000**	Human skin, *ex vivo* indentation	(Geerligs et al., 2011)
	7.80	0.3†	1.500	**0.308**	Human skin, *in vivo* indentation	(Delalleau, 2007)‡[f]
D	0.01	0.3†	**0.001**	**480.000**	Human skin, *in vivo* indentation	(Delalleau, 2007)‡[g]
	0.60	0.30	**0.115**	**4.000**	FE model	(Lévêque & Audoly, 2013) ‡[h]
	0.60	0.50	**0.100**	**0.100**	FE model	(Magnenat-Thalmann et al., 2002)
	0.83	0.3†	0.160	**2.885**	Human skin, suction test	(Hendriks et al., 2006)
	1.00	0.50	**0.167**	**0.060**	FE model	(Magnenat-Thalmann et al., 2002) §
	1.61	0.3†	**0.310**	**1.489**	Human skin, *in vivo* indentation	(Delalleau, 2007)‡[f]

§ Values for aged skin. † Estimated value.

‡ Originally published by:

a - Papir et al. (1975)

b - Pannisset et al. (1994)
c - Dahlgren (1984).
d - Pailler-Mattei and Zahouani (2004)
e - Park (1972).
f - Tran et al. (2005)
g - Lanir et al. (1990)
h - Serup et al. (1995).

Table 2. Design of computational experiment. Mechanical properties of the skin layers implemented in the eight cases/finite element models considered in this study.

Analyses		***Stratum corneum***		**Living Epidermis**			**Dermis**	
		E (MPa)	ν	*E* (MPa)		ν	*E* (MPa)	ν
				A	**B**			
A1	**B1**	0.6	0.3	0.6	0.05	0.3	0.6	0.3
A2	**B2**	370	0.3	0.6	0.05	0.3	0.6	0.3
A3	**B3**	0.6	0.45	0.6	0.05	0.3	0.6	0.3
A4	**B4**	370	0.45	0.6	0.05	0.3	0.6	0.3

Table 3. Fitting function parameters obtained from the logarithmic regression of the furrow depth-strain PVR data. Quality of the correlation is indicated by the coefficient of determination R^2.

Analysis type	**Case**	**m**	**b**	$\mathbf{R^2}$
Compression	A1	14.06	78.94	0.87
	A2	2.52	13.38	0.86
	B1	16.28	77.51	0.91
	B2	1.60	8.33	0.69
Extension	A1	194.19	794.40	0.81
	A2	6.70	31.59	0.91
	B1	53.00	226.33	0.85
	B2	4.91	22.94	0.93

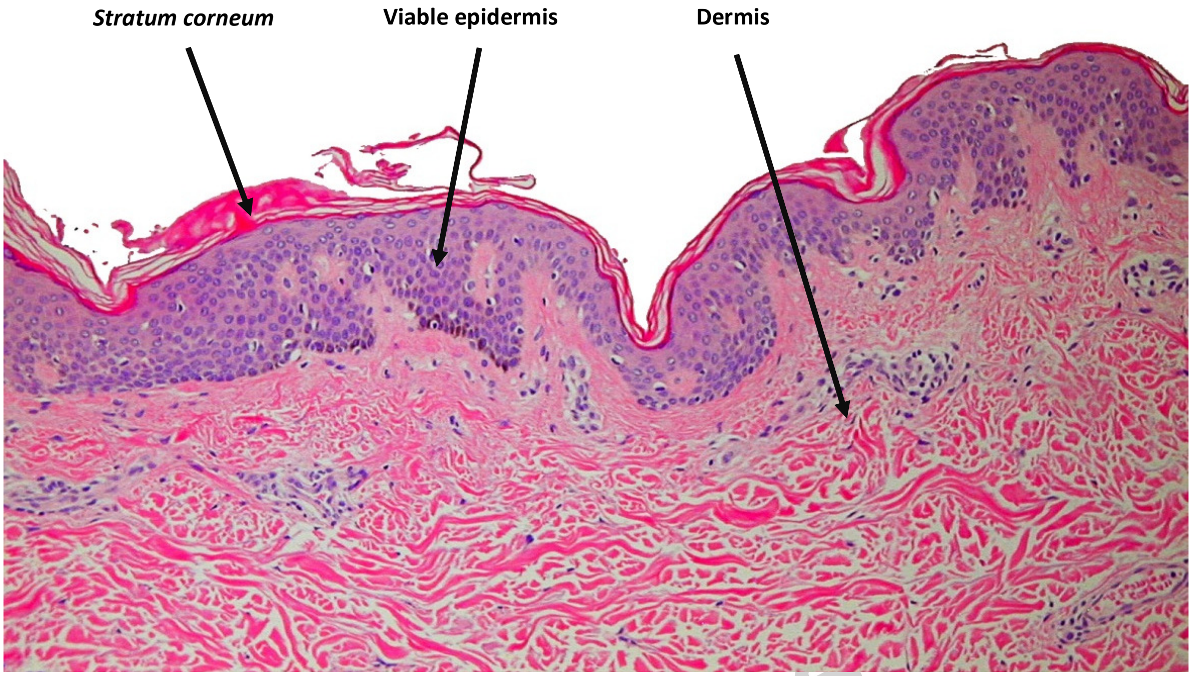

Figure 1. Histological section of human middle back skin, haematoxylin and eosin stained, showing several skin furrows. The *stratum corneum* (SC), viable epidermis (VE) and dermis (D) are clearly visible.

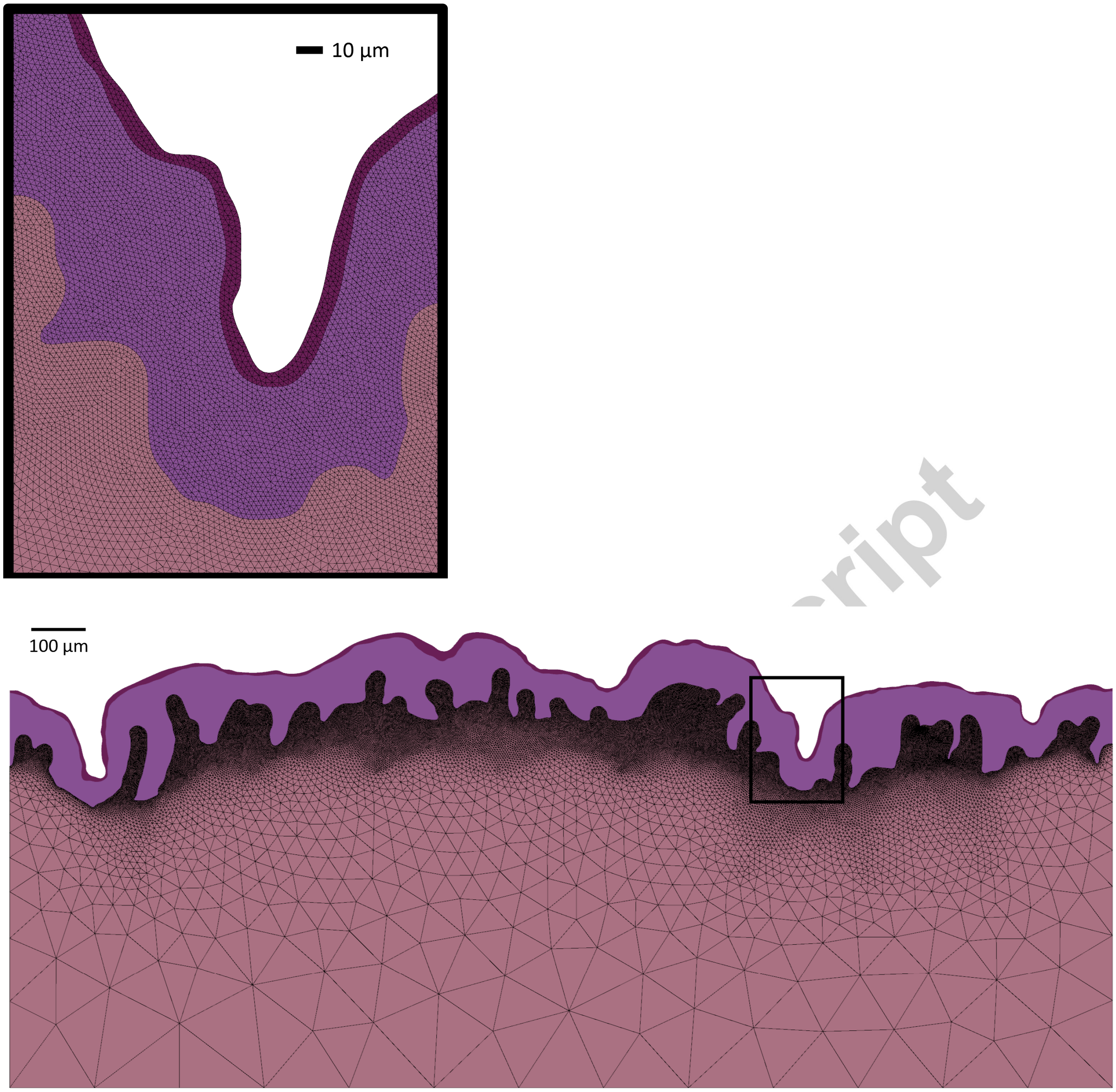

Figure 2. Two-dimensional finite element mesh of the skin histological section with zoomed-in view at the top. For sake of clarity, the edges of the finite elements constituting the *stratum corneum* and viable epidermis are not displayed in the bottom picture.

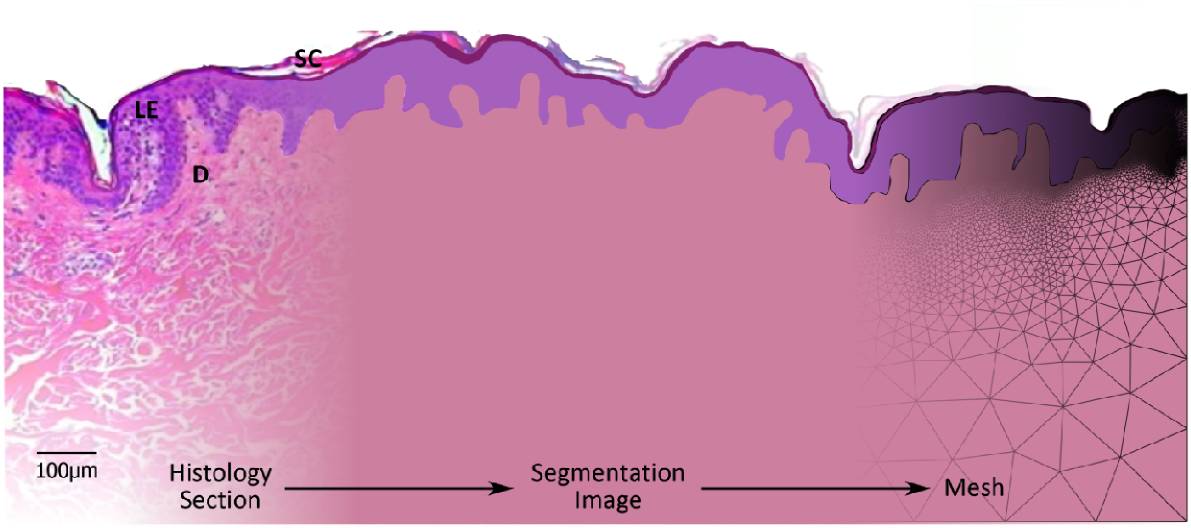

Figure 3. Illustration of the image-based finite element model generation process from histology, image segmentation and mesh generation.

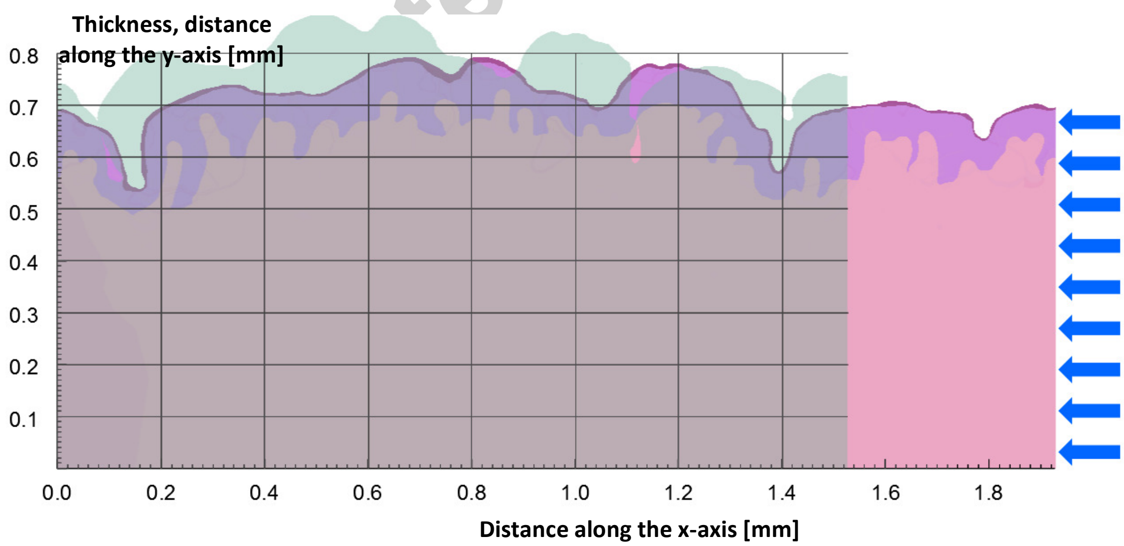

Figure 4. Illustration of the macroscopic loading condition of skin for the compression case (indicated by blue arrows). Vertical displacements are fixed at y = 0 and horizontal displacements are fixed at x = 0. The transparent overlay corresponds to the deformed 2D skin structure after 20±1% deformation.

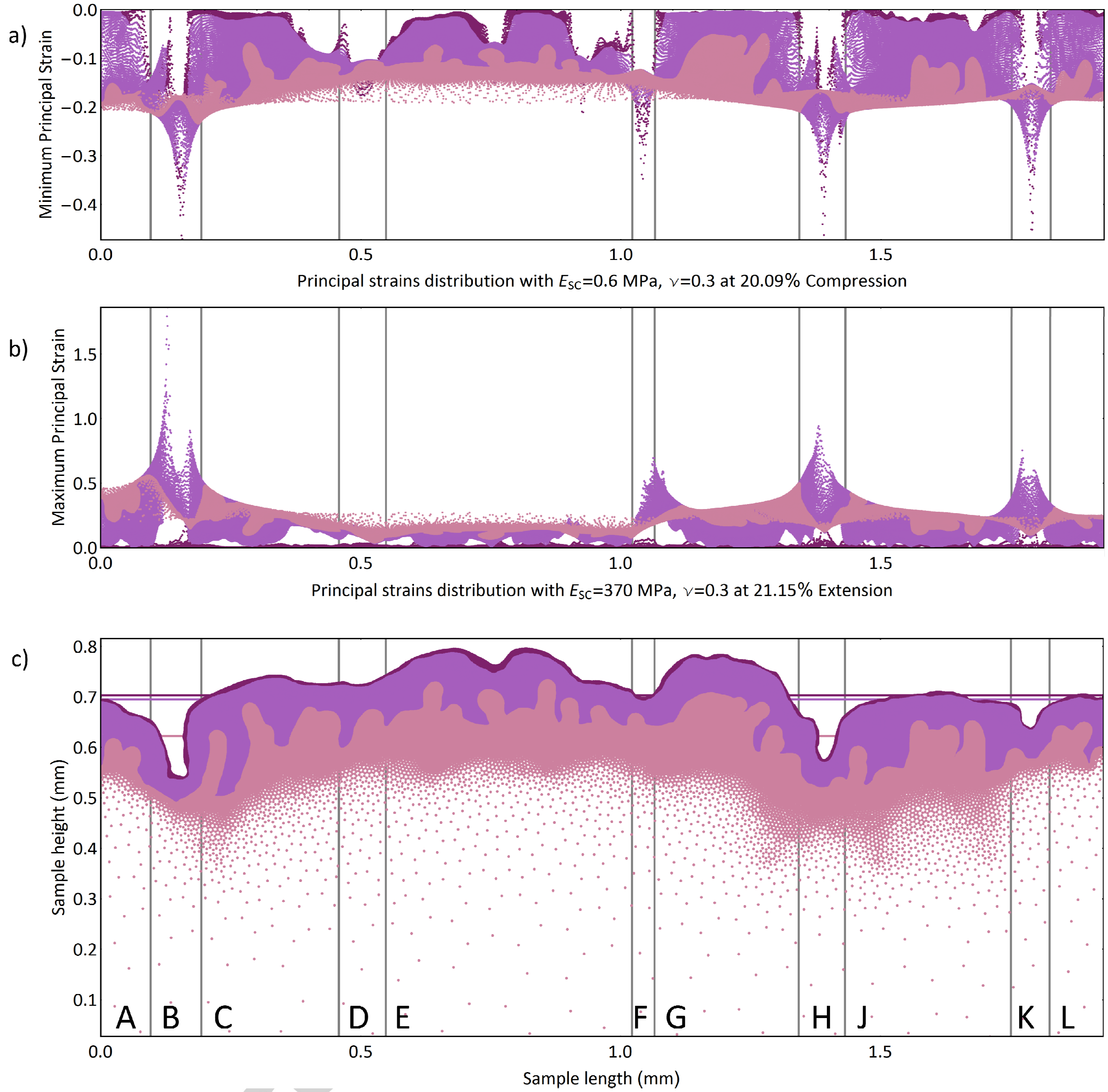

Figure 5. Topographic features of the anatomical multi-layer skin model. These region of interest were selected according to their geometrical characteristics and the magnitude of principal strains for case A1 and A2: (a) in compression (A1) and (b) in extension (A2). These features, which were identified by the letters A-L (omitting letter I), distinguish areas with high strain peaks (skin furrows) from those with small peak strains (crests); (c) plot of the finite elements' centroids in the *stratum corneum* (SC, plum colour), viable epidermis (VE, purple) and dermis (DE, pink). The horizontal lines indicate the mean value of the location of the layer interfaces.

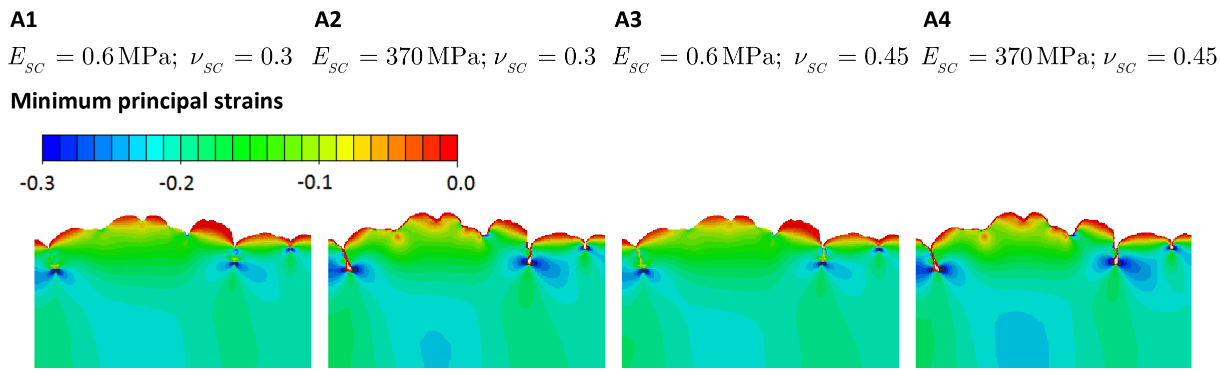

Figure 6. Colour plot of minimum principal strains in the skin for analysis cases A1, A2, A3 and A4 ($E_{LE} = E_{D} = 0.6\,\mathrm{MPa}$ and $\nu_{LE} = \nu_{D} = 0.3$) under simulated **compression**.

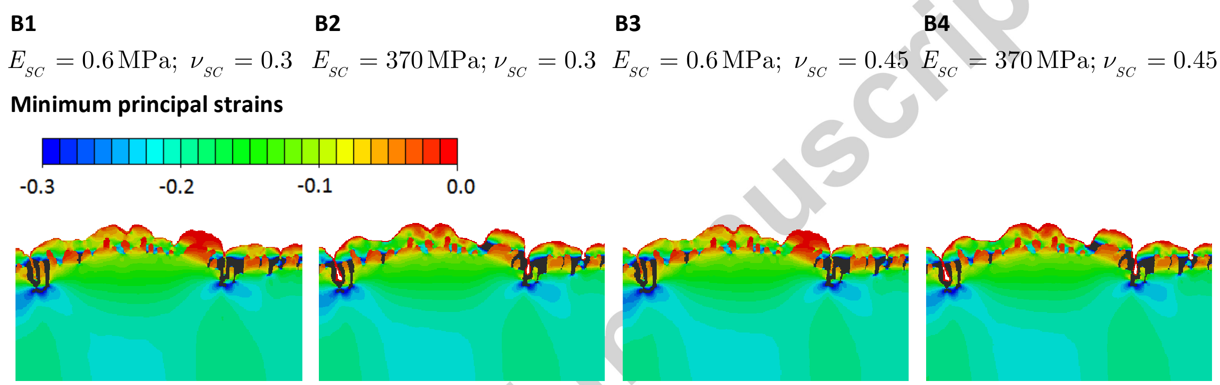

Figure 7. Colour plot of minimum principal strains in the skin for analysis cases B1, B2, B3 and B4 ($E_{LE} = 0.05\,\mathrm{MPa}$, $E_{D} = 0.6\,\mathrm{MPa}$ and $\nu_{LE} = \nu_{D} = 0.3$) under simulated **compression**.

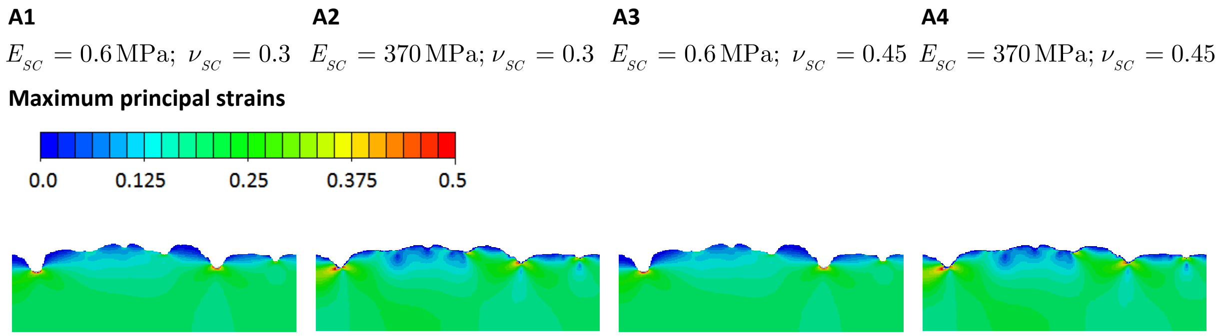

Figure 8. Colour plot of maximum principal strains in the skin for analysis cases A1, A2, A3 and A4 ($E_{LE} = E_{D} = 0.6\,\mathrm{MPa}$ and $\nu_{LE} = \nu_{D} = 0.3$) under simulated **extension**.

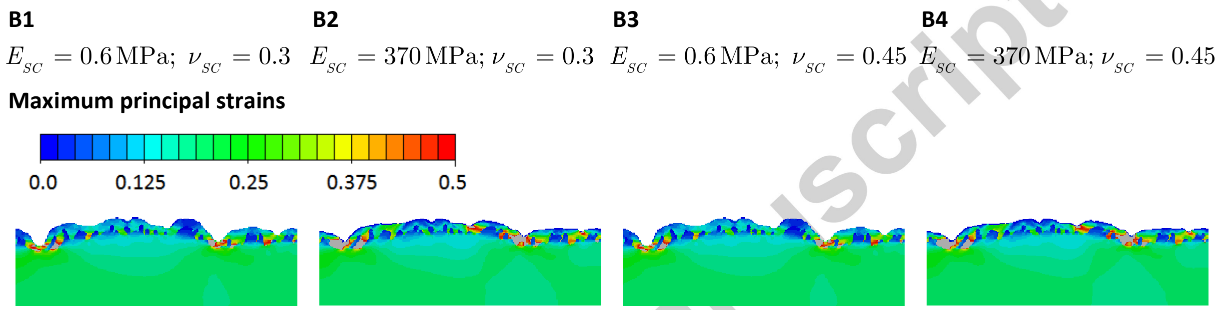

Figure 9. Colour plot of maximum principal strains in the skin for analysis cases B1, B2, B3 and B4 ($E_{LE} = 0.05\,\mathrm{MPa}$, $E_{D} = 0.6\,\mathrm{MPa}$ and $\nu_{LE} = \nu_{D} = 0.3$) under simulated **extension**.

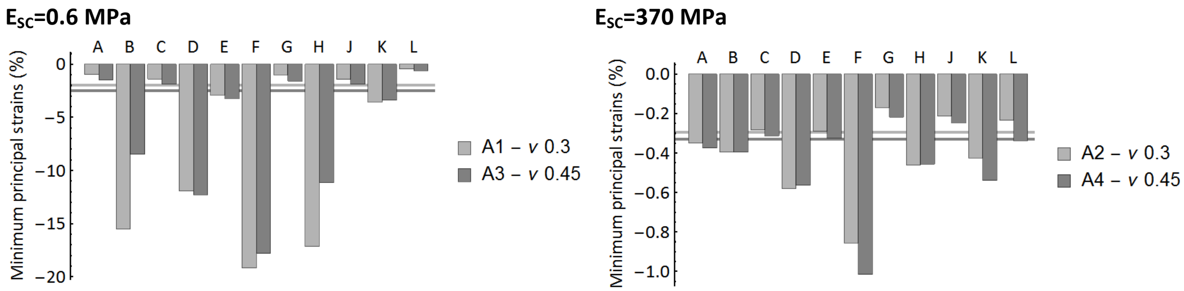

Figure 10. Bar chart representing local median **minimum** principal strain (LMS) values in the *stratum corneum* at each characteristic skin topographic zone (A, B, C, D, E, F, G, H, J, K and L, **Figure 5**) for cases A1, A2, A3 and A4 (in **compression**). The horizontal lines correspond to the global median principal strain values (GMS) of the whole *stratum corneum* (GMS).

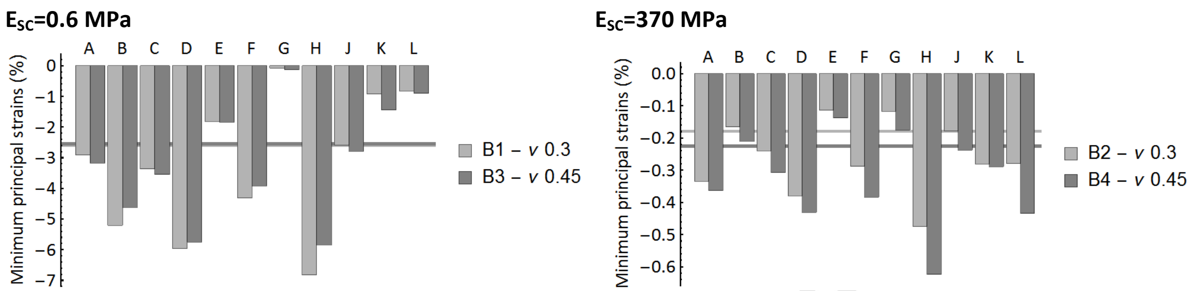

Figure 11. Bar chart representing local median **minimum** principal strain (LMS) values in the *stratum corneum* at each characteristic skin topographic zone (A, B, C, D, E, F, G, H, J, K and L, **Figure 5**) for cases B1, B2, B3 and B4 (in **compression**). The horizontal lines correspond to the global median principal strain values (GMS) of the whole *stratum corneum* (GMS).

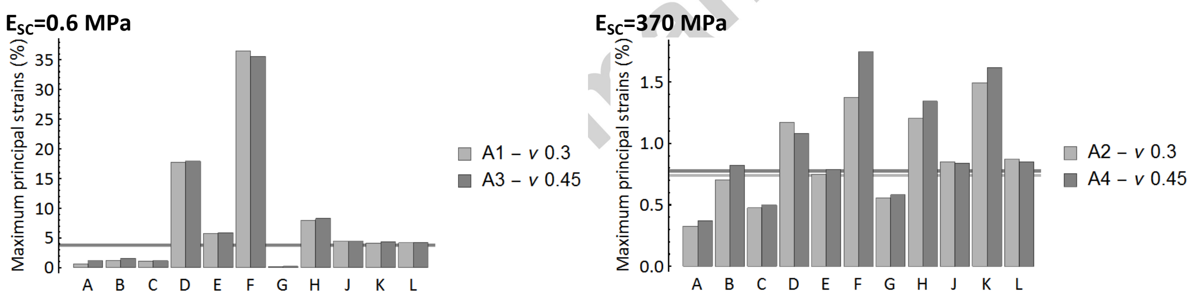

Figure 12. Bar chart representing local median **maximum** principal strain (LMS) values in the *stratum corneum* at each characteristic skin topographic zone (A, B, C, D, E, F, G, H, J, K and L, **Figure 5**) for cases A1, A2, A3 and A4 (in **extension**). The horizontal lines correspond to the global median principal strain values (GMS) of the whole *stratum corneum* (GMS).

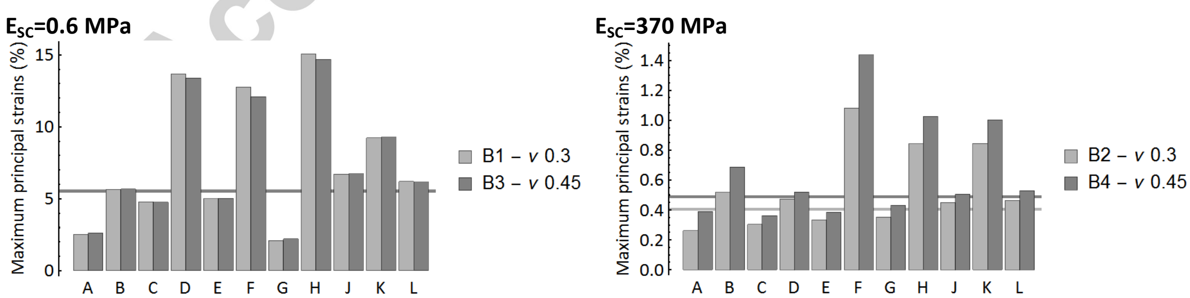

Figure 13. Bar chart representing local median **maximum** principal strain (LMS) values in the *stratum corneum* at each characteristic skin topographic zone (A, B, C, D, E, F, G, H, J, K and L, **Figure 5**) for cases B1, B2, B3 and B4 (in **extension**). The horizontal lines correspond to the global median principal strain values (GMS) of the whole *stratum corneum* (GMS).

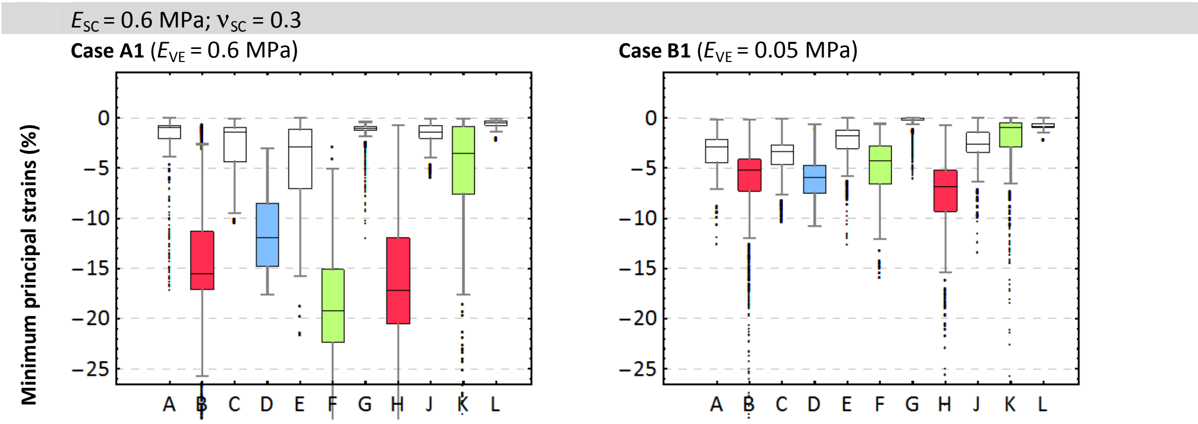

Figure 14. Box plot representing the minimum principal strains distributions in the *stratum corneum* across the different topographic features of the skin (zone A to L, **Figure 5**) under **compression**. Minimum principal strains are presented for cases A1 (where the viable epidermis and dermis share the same mechanical properties) and B1 (where the viable epidermis is 12 times softer than the dermis).

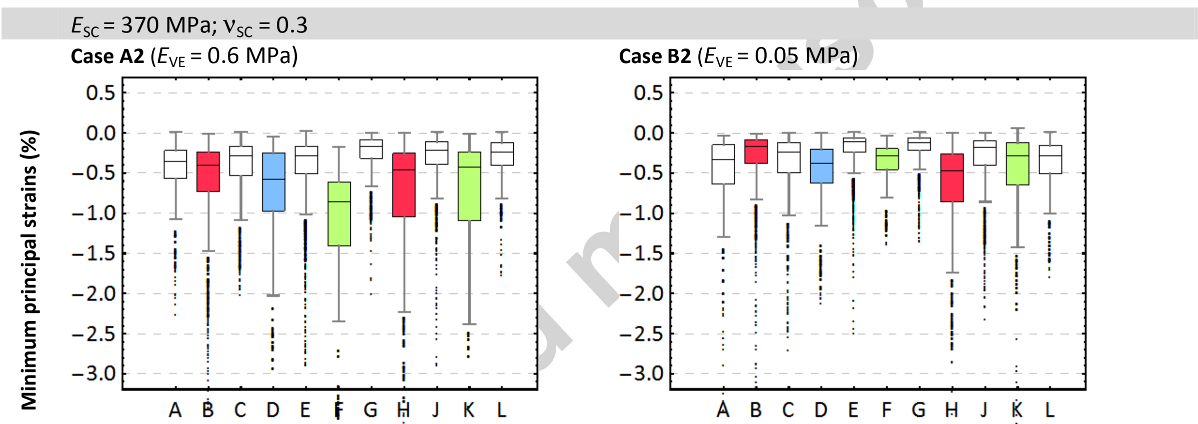

Figure 15. Box plot representing the minimum principal strains distributions in the *stratum corneum* across the different topographic features of the skin (zone A to L, **Figure 5**) under **compression**. Minimum principal strains are presented for cases A2 (where the viable epidermis and dermis share the same mechanical properties) and B2 (where the viable epidermis is 12 times softer than the dermis).

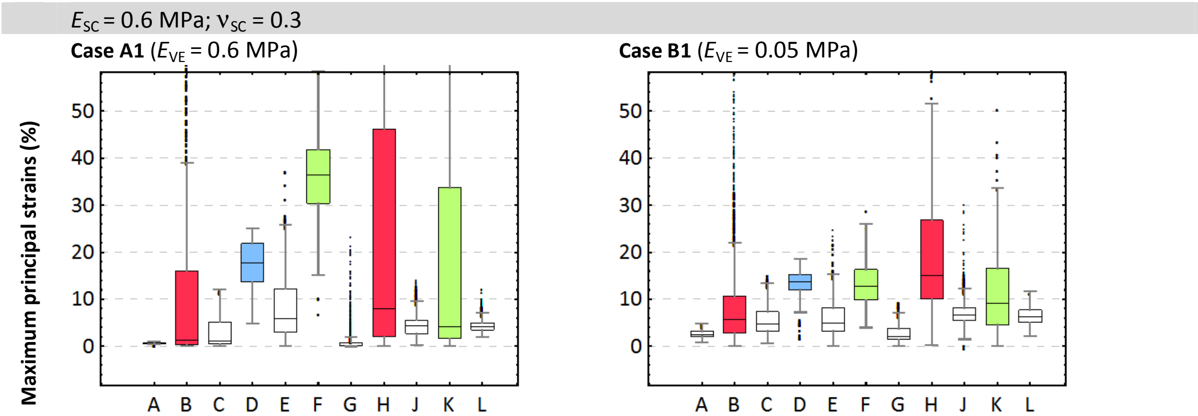

Figure 16. Box plot representing the minimum principal strains distributions in the *stratum corneum* across the different topographic features of the skin (zone A to L, **Figure 5**) under **extension**. Minimum principal strains are presented for cases A1 (where the viable epidermis and dermis share the same mechanical properties) and B1 (where the viable epidermis is 12 times softer than the dermis).

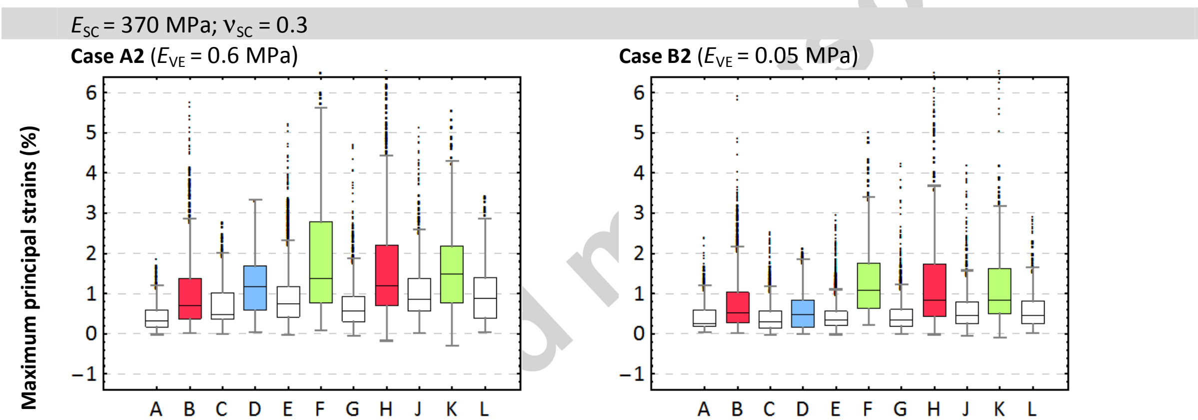

Figure 17. Box plot representing the minimum principal strains distributions in the *stratum corneum* across the different topographic features of the skin (zone A to L, **Figure 5**) under **compression**. Minimum principal strains are presented for cases A2 (where the viable epidermis and dermis share the same mechanical properties) and B2 (where the viable epidermis is 12 times softer than the dermis).

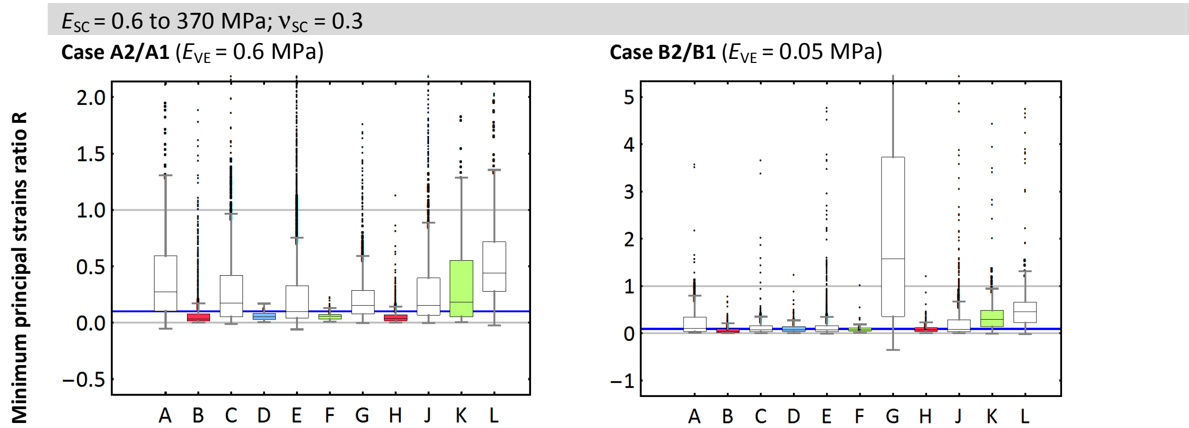

Figure 18. Box plot representing the distribution of ratio of minimum principal strains from analysis A2 (ESC = 370 MPa, ν = 0.3) over those of analysis A1 (ESC = 0.6 MPa, ν = 0.3) in the *stratum corneum* across the different topographic features of the skin (zone A to L, **Figure 6**) under **compression**. The same ratio of strains from analysis B2 over those of analysis B1 when the Young's modulus of the viable epidermis is 0.05 MPa is also plotted. The values between 0 and 1 (grey lines) represent a reduction in principal strains while the values higher than one represent amplification. The blue horizontal line indicates the median value of the ratio obtained for all the elements of the *stratum corneum* in the skin model (i.e. the general median strain ratio, GMS ratio).

Minimum principal strains are presented for cases A**2** (where the viable epidermis and dermis share the same mechanical properties) and B**2** (where the viable epidermis is 12 times softer than the dermis).

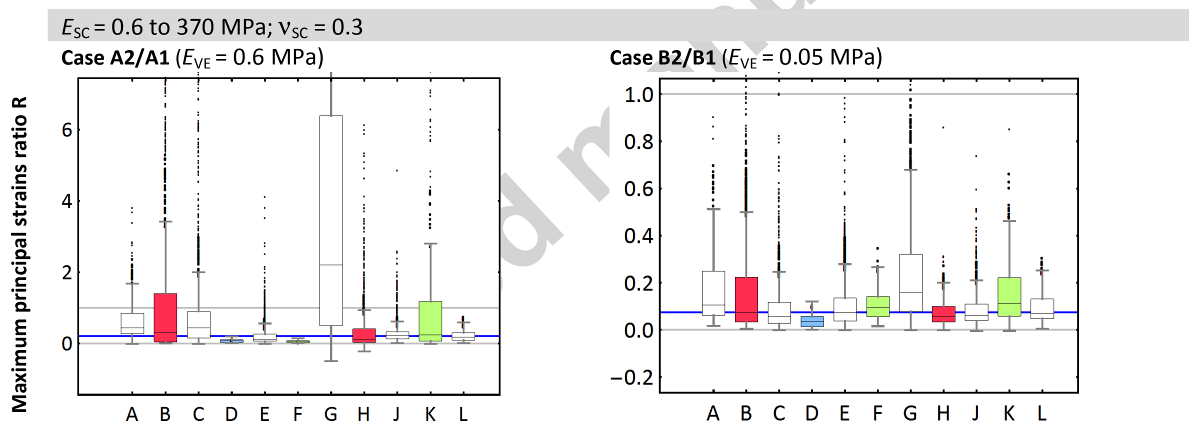

Figure 19. Box plot representing the distribution of ratio of minimum principal strains from analysis A2 (ESC = 370 MPa, ν = 0.3) over those of analysis A1 (ESC = 0.6 MPa, ν = 0.3) in the *stratum corneum* across the different topographic features of the skin (zone A to L, **Figure 6**) under **extension**. The same ratio of strains from analysis B2 over those of analysis B1 when the Young's modulus of the viable epidermis is 0.05 MPa is also plotted. The values between 0 and 1 (grey lines) represent a reduction in principal strains while the values higher than one represent amplification. The blue horizontal line indicates the median value of the ratio obtained for all the elements of the *stratum corneum* in the skin model (i.e. the general median strain ratio, GMS ratio).

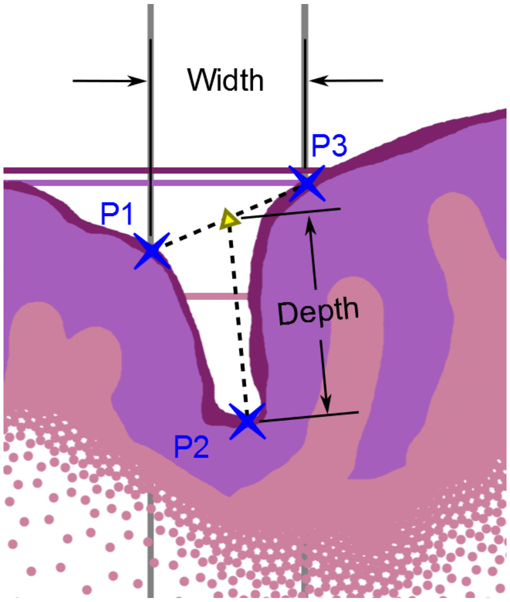

Figure 20. Schematic illustrating the characteristic dimensions of a skin furrow (depth and width). By selecting three points defining the location of the furrow edges (P1, P3) and the deepest point (P2) of the furrow (blue crosses), the width was determined by the horizontal distance between P1 and P3, and the depth as the distance between the midpoint between P1 and P3 and P2.

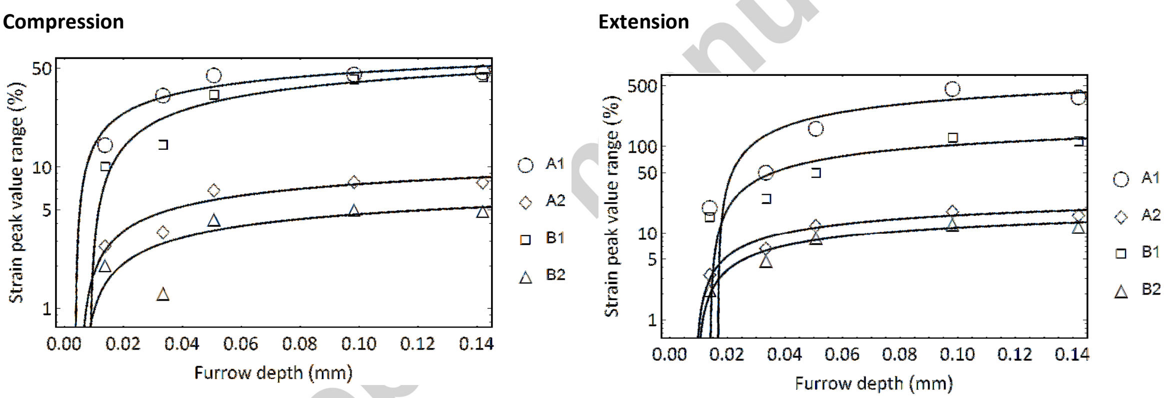

Figure 21. Plot representing the regression analysis between furrow depth and the principal strain peak value range (PVR) experienced by the *stratum corneum* layer under compression (left) and extension (right). The continuous lines represent the best fit using a logarithmic regression.

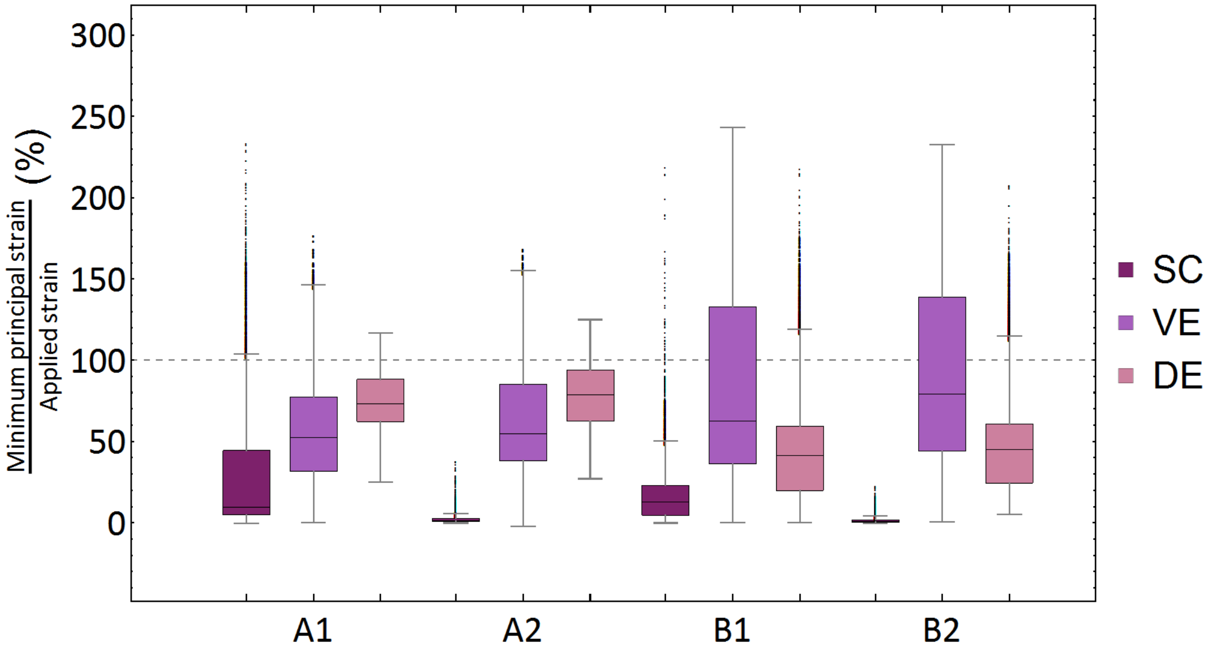

Figure 22. Ratio of minimum principal strains in each skin layer (SC – *stratum corneum*, VE – viable epidermis, DE - dermis) over the macroscopic strain applied to the skin composite model (expressed in %) for the **compression** case. The dashed line indicates the limit between strain amplification (> 100 %) and strain reduction (< 100 %).

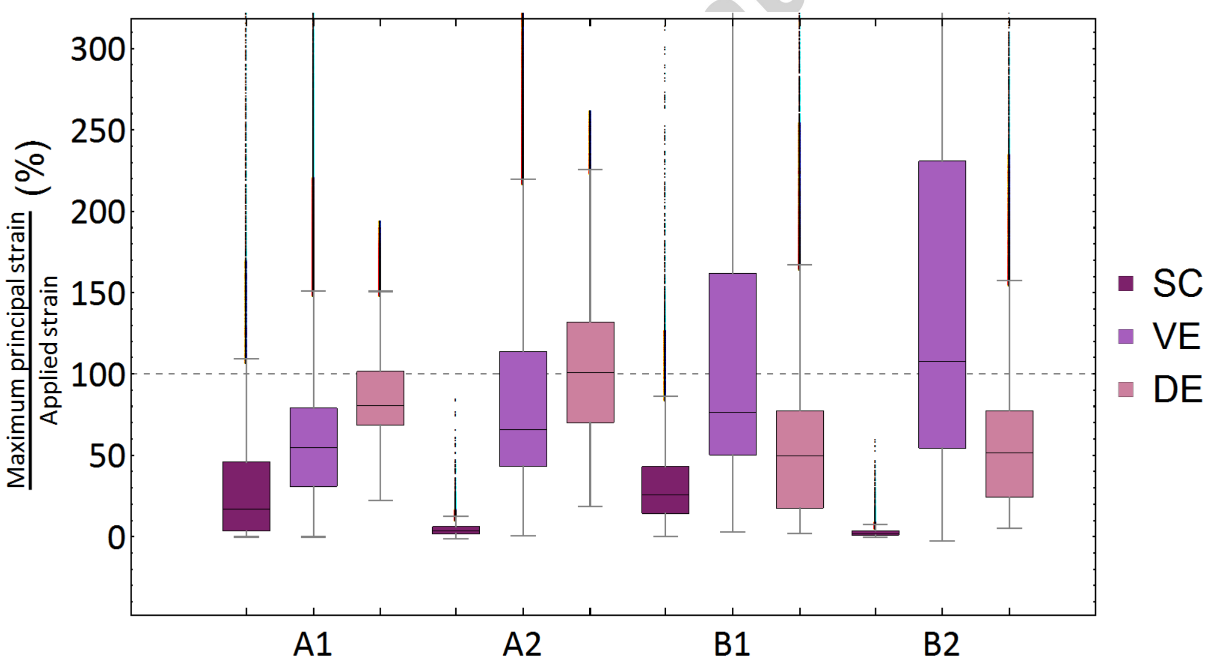

Figure 23. Ratio of minimum principal strains in each skin layer (SC – *stratum corneum*, VE – viable epidermis, DE - dermis) over the macroscopic strain applied to the skin composite model (expressed in %) for the **extension** case. The dashed line indicates the limit between strain amplification (> 100 %) and strain reduction (< 100 %).

Graphical Abstract (for review)